Electronic Supporting Information for

Transition Metal Complexes of the (2,2,2-Trifluoroethyl)phosphinate NOTA Analogue as Potential Contrast Agents for ^{19}F Magnetic Resonance Imaging

Filip Koucký,[a] Tereza Dobrovolná,[a] Jan Kotek,[a,*] Ivana Císařová,[a] Jana Havlíčková,[a] Alan Liška,[b] Vojtěch Kubíček[a] and Petr Hermann[a]

[a] Department of Inorganic Chemistry, Faculty of Science, Charles University, Hlavova 8, 128 42 Prague 2, Czech Republic. E-mail: modrej@natur.cuni.cz.

[b] Department of Molecular Electrochemistry and Catalysis, J. Heyrovský Institute of Physical Chemistry AS CR, Dolejškova 2155/3, 182 23 Prague 8, Czech Republic.

Contents

Schematic representation of HPLC method used for characterizations

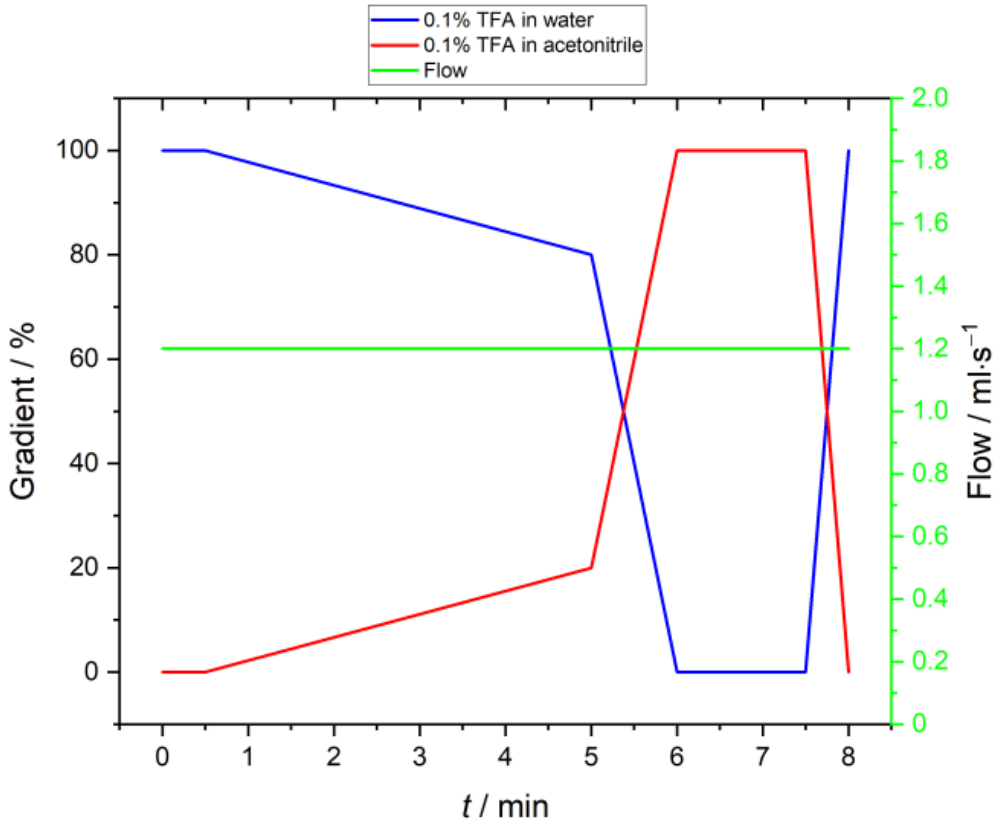

Figure S1. Gradient method used for characterization of H_3notp^{tfe} and its complexes.

Apparatus for synthesis of 2,2,2-trifluoroethylbromide

Figure S2. Reaction apparatus for synthesis of 2,2,2-trifluoroethylbromide.

HPLC-MS chromatogram of H_3notp^{tfe}

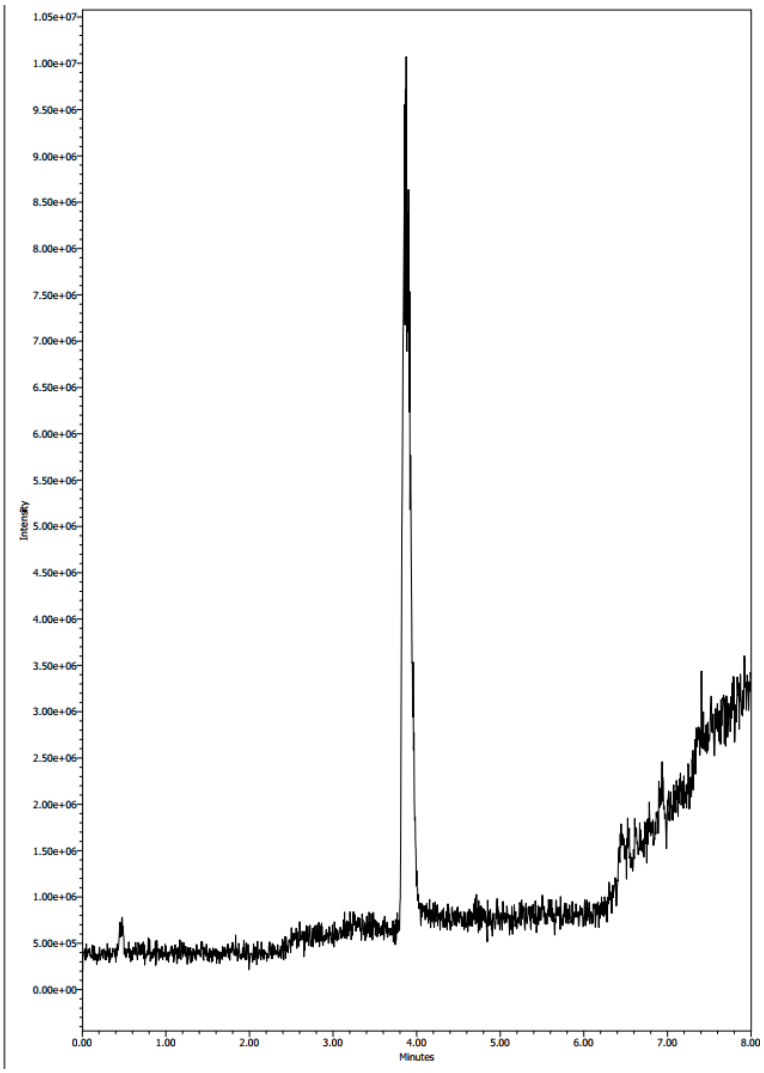

Figure S3. HPLC chromatogram of H_3notp^{tfe} with MS detection (total ion current shown of *y*-axis) using the method shown in Figure S1.

NMR spectra of H_3notp^{tfe}

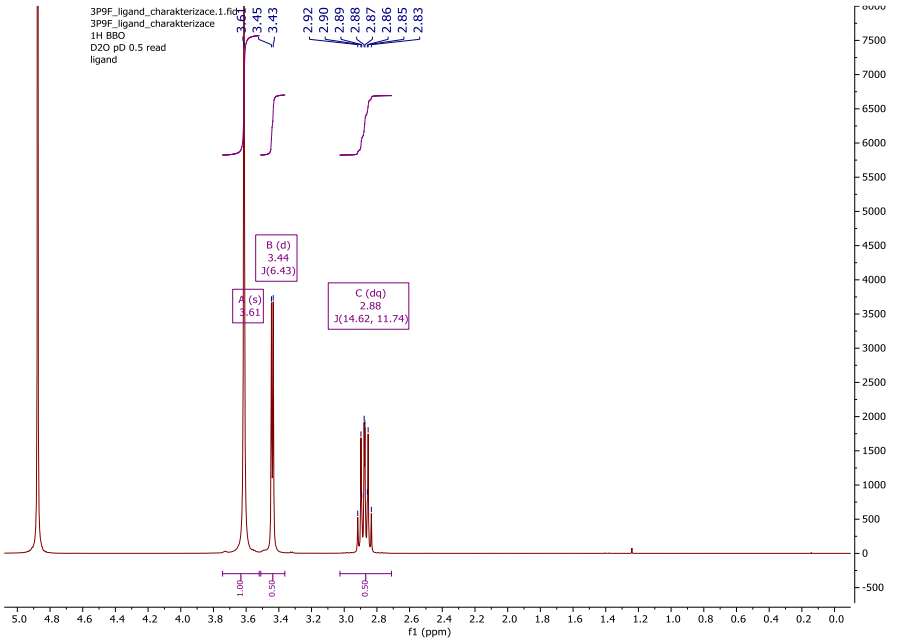

Figure S4. ^{1}H NMR spectrum of H_3notp^{tfe} (D_2O, pD 0.5).

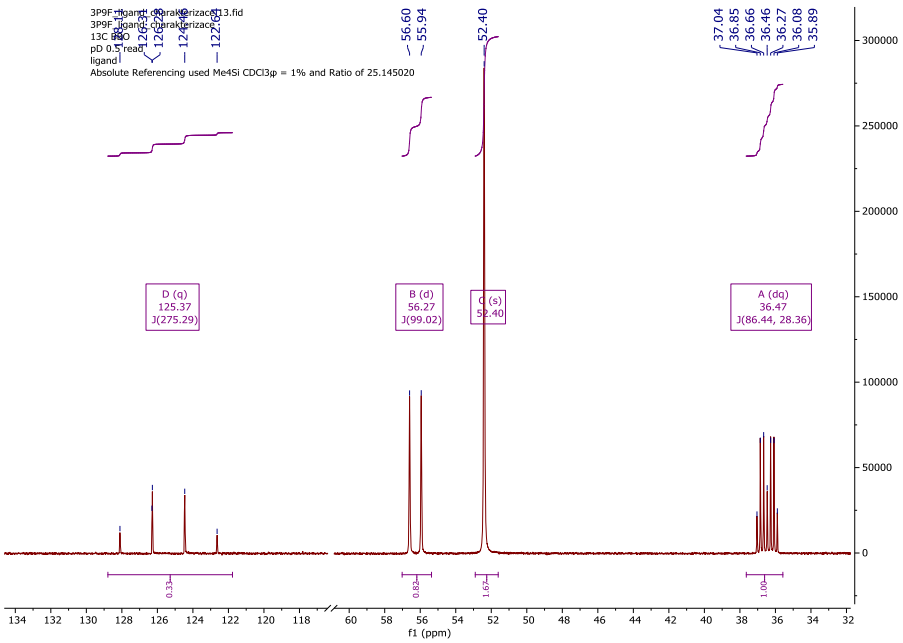

Figure S5. $^{13}C\{^{1}H\}$ NMR spectrum of H_3notp^{tfe} (D_2O, pD 0.5).

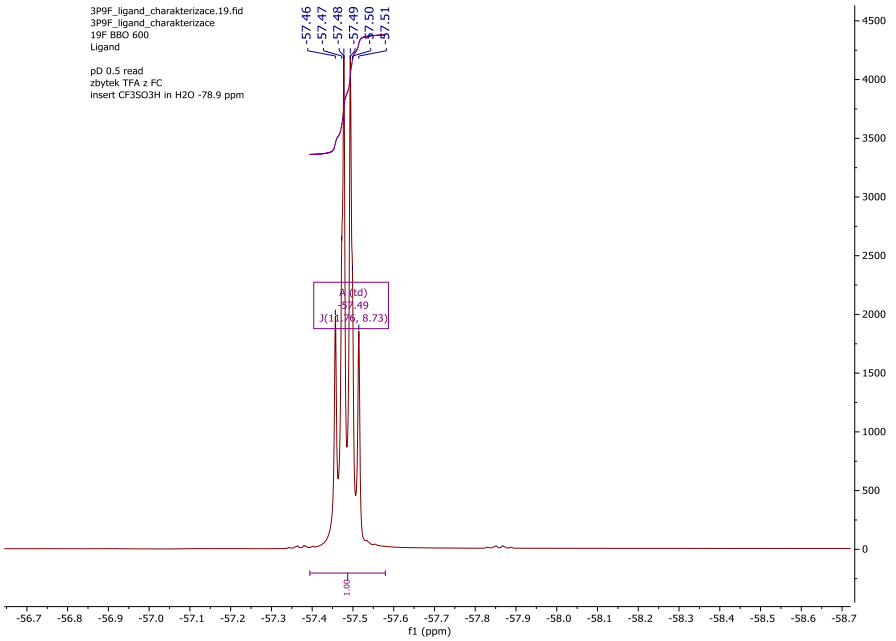

Figure S6. ^{19}F NMR spectrum of H_3notp^{tfe} (D_2O, pD 0.5).

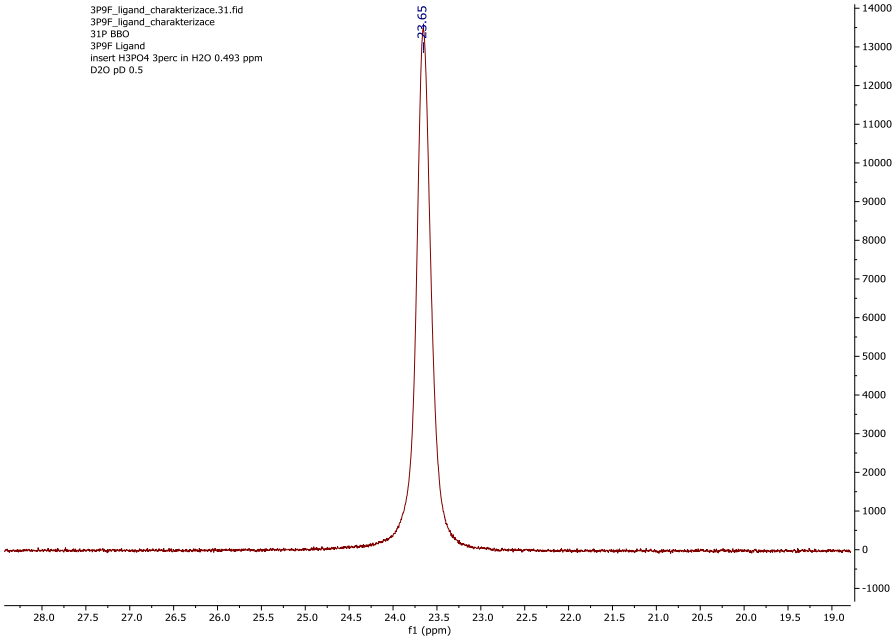

Figure S7. ^{31}P NMR spectrum of H_3notp^{tfe} (D_2O, pD 0.5).

Selected NMR and UV-Vis spectra of M^{2+}–H_3notp^{tfe} complexes

Table S1. Observed ^{19}F NMR chemical shift of H_3notp^{tfe} and the studied complexes, reduction for bulk magnetic susceptibility effect, and the corrected chemical shifts. Signal of 2,2,2-trifluoroethanol was used for the correction.

Sample	Observed δ / ppm	$\Delta\delta$(BMS)	Corrected δ / ppm
H_3notp^{tfe}	−57.12	0	−57.12 (m)
Mg^{2+}–H_3notp^{tfe} system	−57.30	0	−57.30 (br. q, J = 10 Hz)
$[Cr^{III}(notp^{tfe})]$	−45.5	0.51	−46.0
$[Mn^{II}(notp^{tfe})]^-$	−39.9	1.93	−41.8
$[Fe^{III}(notp^{tfe})]$	−28.8	2.24	−31.0
$[Co^{II}(notp^{tfe})]^-$	−49.1	1.44	−50.5
$[Ni^{II}(notp^{tfe})]^-$	−47.8	0.74	−48.5
$[Cu^{II}(notp^{tfe})]^-$	−53.7	0.46	−54.2
$[Zn^{II}(notp^{tfe})]^-$	−57.21	0	−57.21 (“q”, J = 10.5 Hz)

Table S2. Half-widths (Hz) of ^{19}F NMR signals of the studied complexes (MestRenova 12.0.3).

	565 MHz		376 MHz		282 MHz	
Complex	25 °C	37 °C	25 °C	37 °C	25 °C	37 °C
$[Cr^{III}(notp^{tfe})]$	~$2\cdot10^3$ [a]	~$2\cdot10^3$ [a]	– [b]	– [b]	– [b]	– [b]
$[Mn^{II}(notp^{tfe})]^-$	~$6\cdot10^3$ [a]	~$5\cdot10^3$ [a]	– [b]	– [b]	– [b]	– [b]
$[Fe^{III}(notp^{tfe})]$	$1.51\cdot10^3$	$1.22\cdot10^3$	$1.48\cdot10^3$	$1.16\cdot10^3$	$1.34\cdot10^3$	$1.07\cdot10^3$
$[Co^{II}(notp^{tfe})]^-$	179	314	153	244	140	195
$[Ni^{II}(notp^{tfe})]^-$	169	138	154	124	136	120
$[Cu^{II}(notp^{tfe})]^-$	152	124	177	144	187	145

[a] Only a rough estimate due to very fast relaxation. [b] Spectra cannot be successfully phased.

Mg^{2+}–H_3notp^{tfe} system

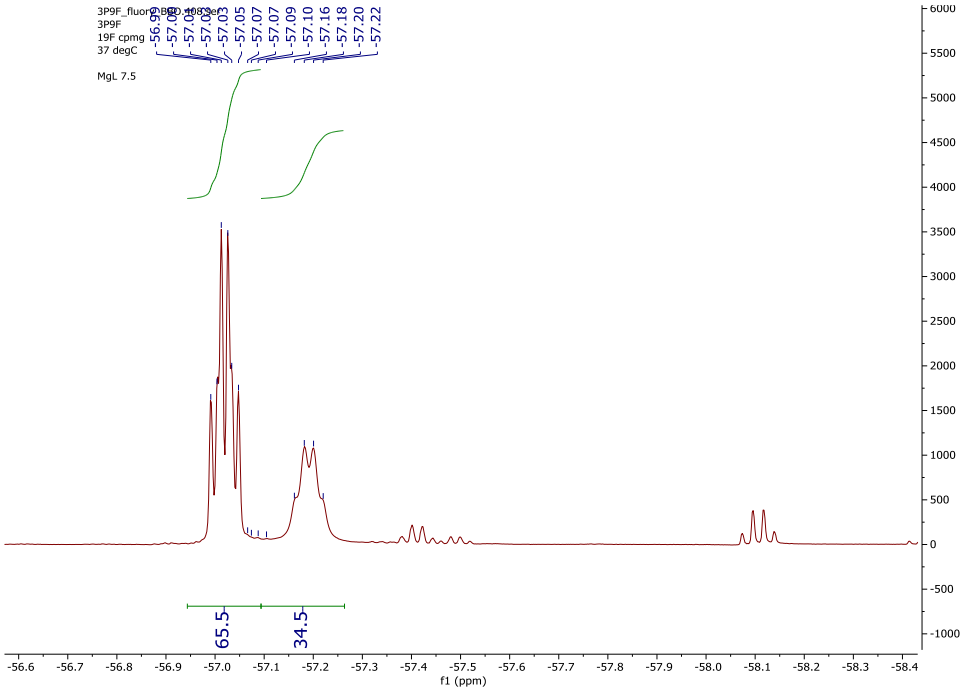

Figure S8. ^{19}F NMR spectra of the Mg^{2+}–H_3notp^{tfe} system (H_2O, pH 7.5, 37 °C, 565 MHz).

$[Cr^{III}(notp^{tfe})]$

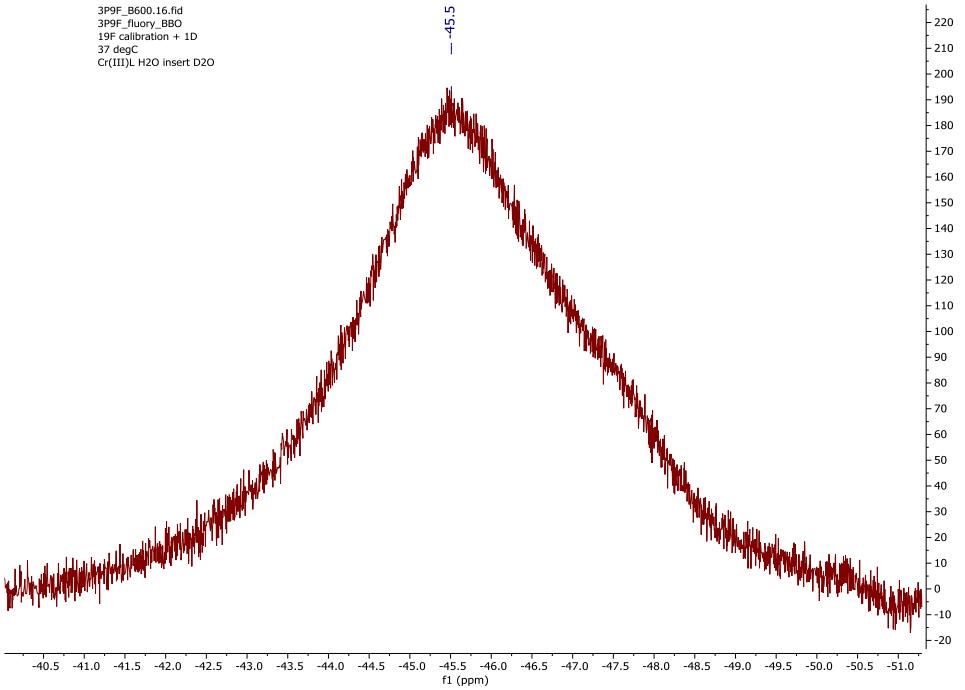

Figure S9. ^{19}F NMR spectra of $[Cr^{III}(notp^{tfe})]$ (H_2O, pH 7.4, 37 °C, 565 MHz).

[Mn^{II}(notp^{tfe})]$^{-}$

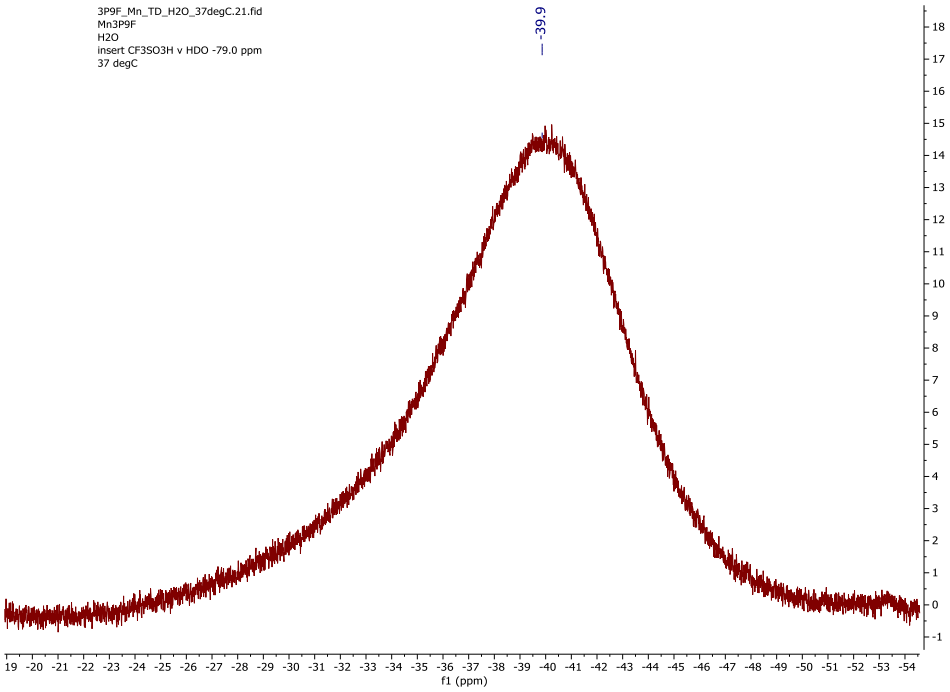

Figure S10. ^{19}F NMR spectra of [Mn^{II}(notp^{tfe})]$^{-}$ (H_2O, pH 7.4, 37 °C, 565 MHz).

[Fe^{III}(notp^{tfe})]

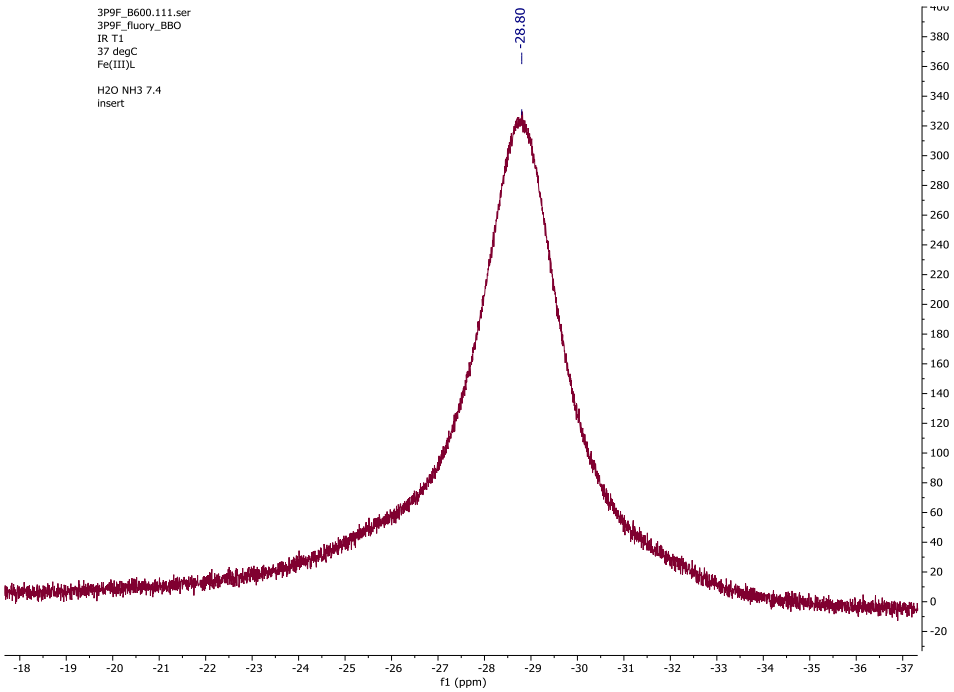

Figure S11. ^{19}F NMR spectra of [Fe^{III}(notp^{tfe})] (H_2O, pH 7.4, 37 °C, 565 MHz).

$[Co^{II}(notp^{tfe})]^-$

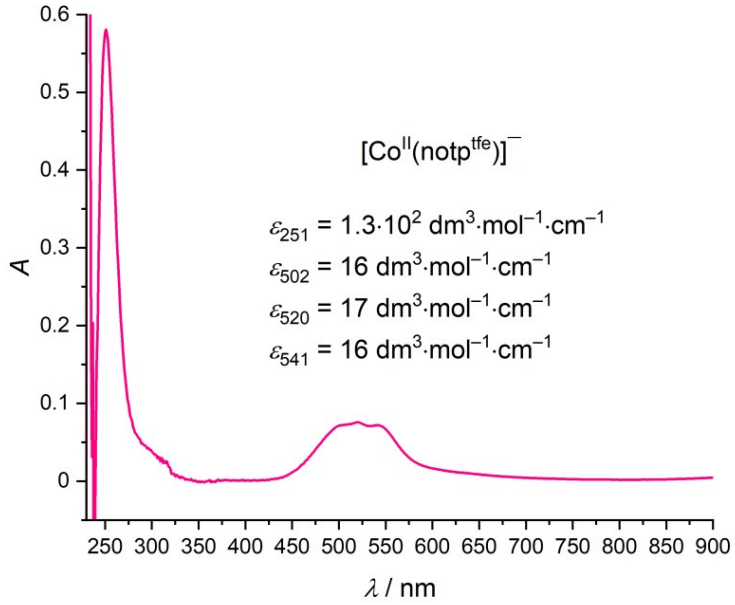

Figure S12. UV-Vis spectrum of $[Co^{II}(notp^{tfe})]^-$ (HEPES, pH 7.4).

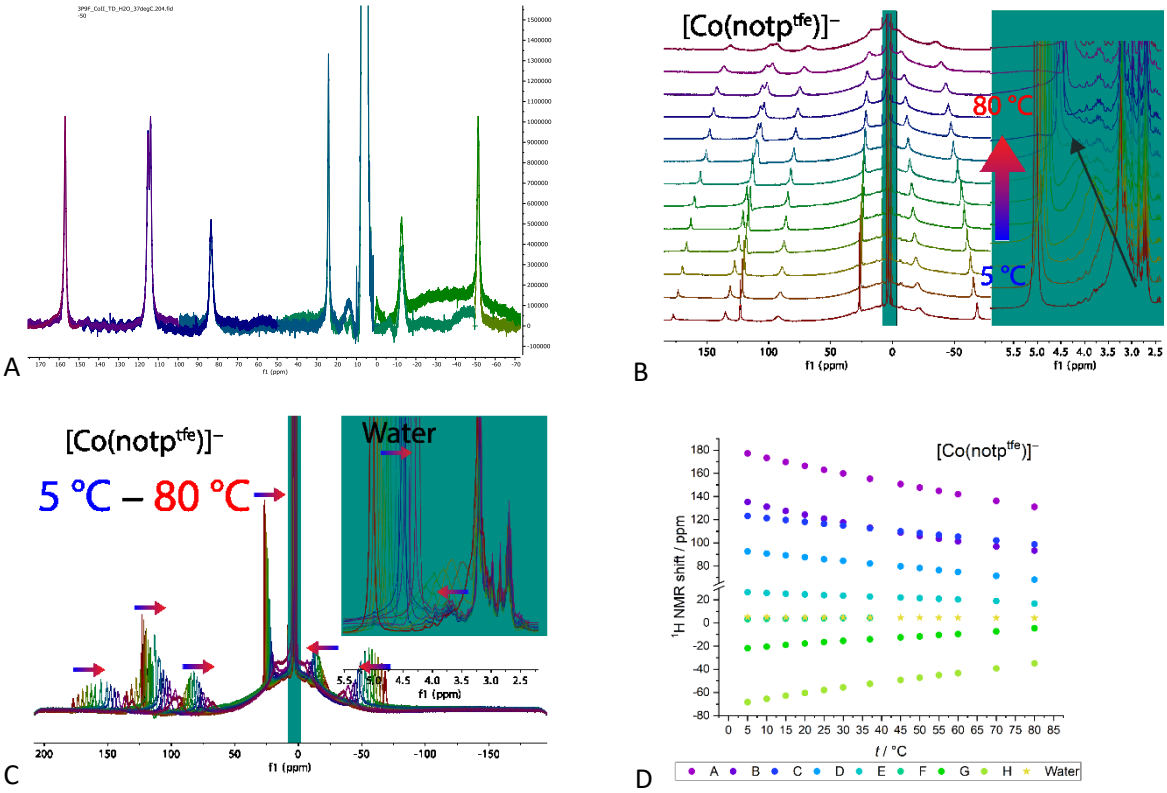

Figure S13. a) ^{1}H NMR spectrum of $[Co^{II}(notp^{tfe})]^-$ (D_2O, pD = 7.4, 37 °C, 600 MHz). Parts of the spectrum obtained with different offsets are highlighted by use of different colours. b) Temperature dependence of the spectra; the inset shows appearance of the "missing" signal which overlaps with diamagnetic "impurities" (ligand excess, $[Co^{III}(notp^{tfe})]$) and water/HDO. c) Temperature dependence of the spectra, arrows show change of chemical shifts. d) Chemical shift changes of individual signals.

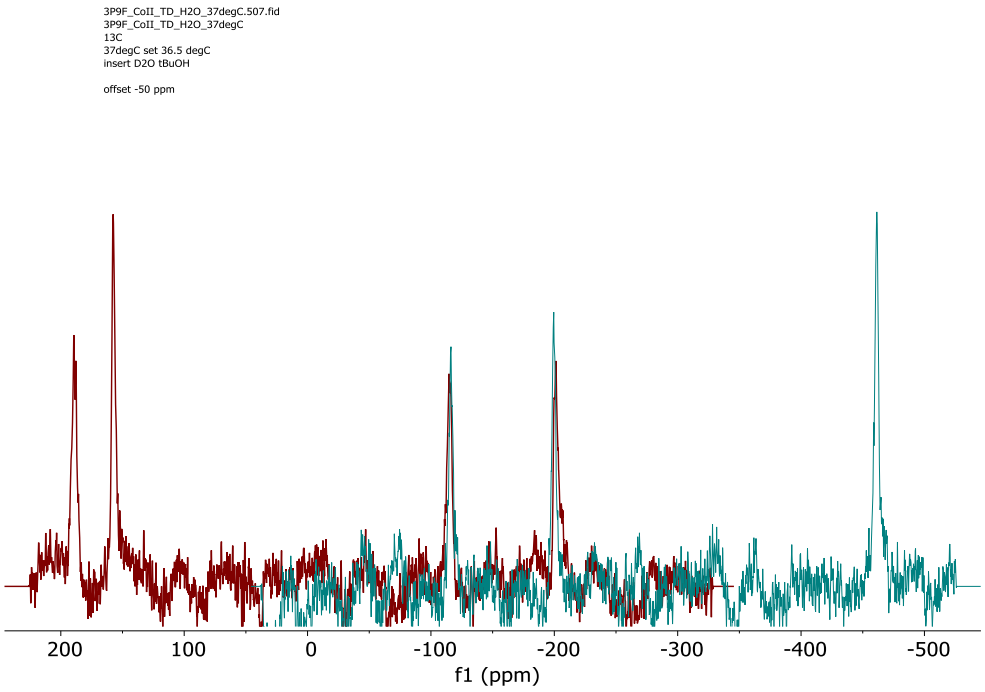

Figure S14. $^{13}C\{^{1}H\}$ NMR spectra of $[Co^{II}(notp^{tfe})]^{-}$ (D_2O, pD 7.4, 37 °C, 151 MHz). Parts of the spectrum obtained with different offsets are highlighted by use of different colours.

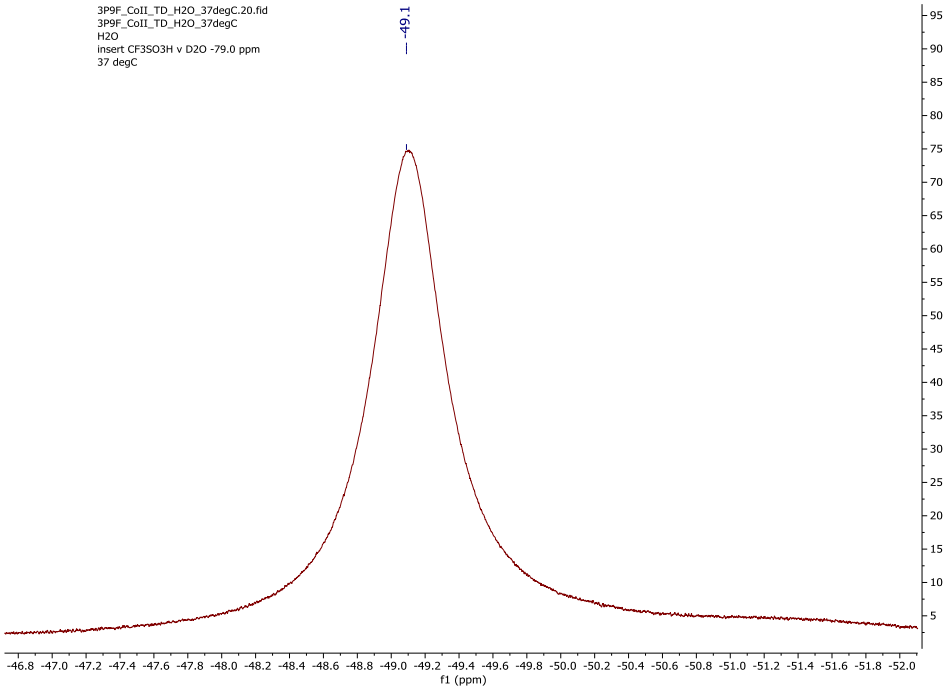

Figure S15. ^{19}F NMR spectra of $[Co^{II}(notp^{tfe})]^{-}$ (D_2O, pD 7.4, 37 °C, 565 MHz).

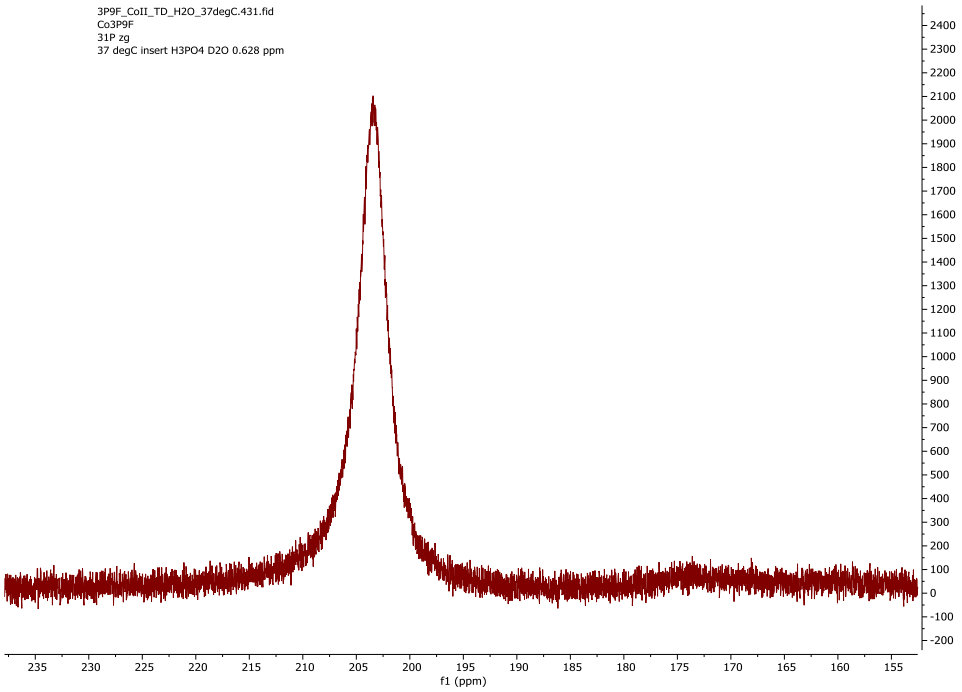

Figure S16. ^{31}P NMR spectra of $[Co^{II}(notp^{tfe})]^-$ (D_2O, pD 7.4, 37 °C, 242 MHz).

$[Ni^{II}(notp^{tfe})]^-$

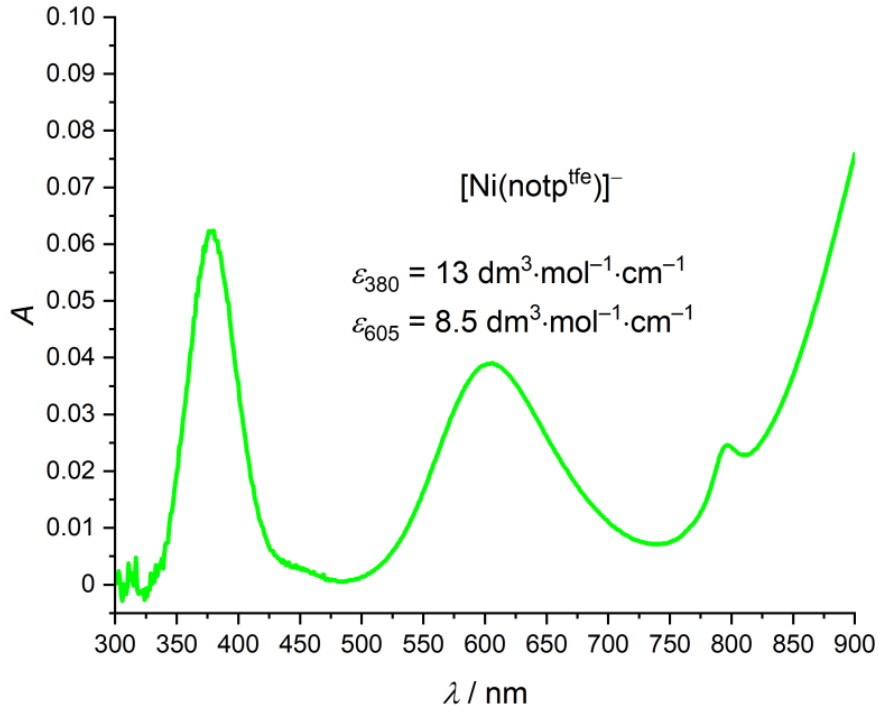

Figure S17. UV-Vis spectrum of $[Ni^{II}(notp^{tfe})]^-$ (HEPES, pH 7.4).

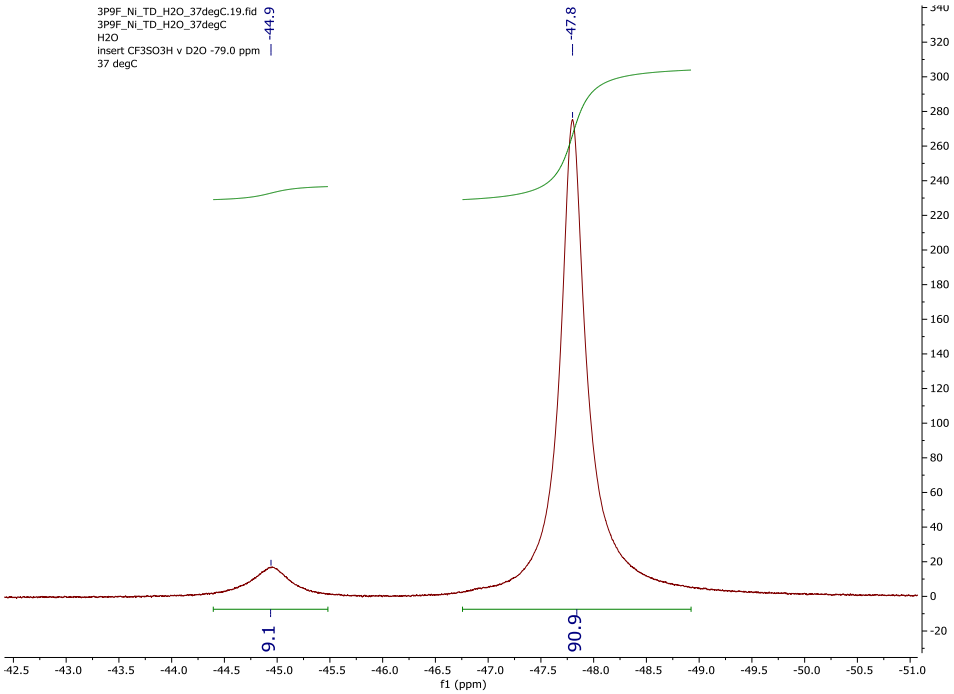

Figure S18. ^{19}F NMR spectra of $[Ni^{II}(notp^{tfe})]^-$ (D_2O, pD 7.4, 37 °C, 565 MHz).

$[Cu^{II}(notp^{tfe})]^-$

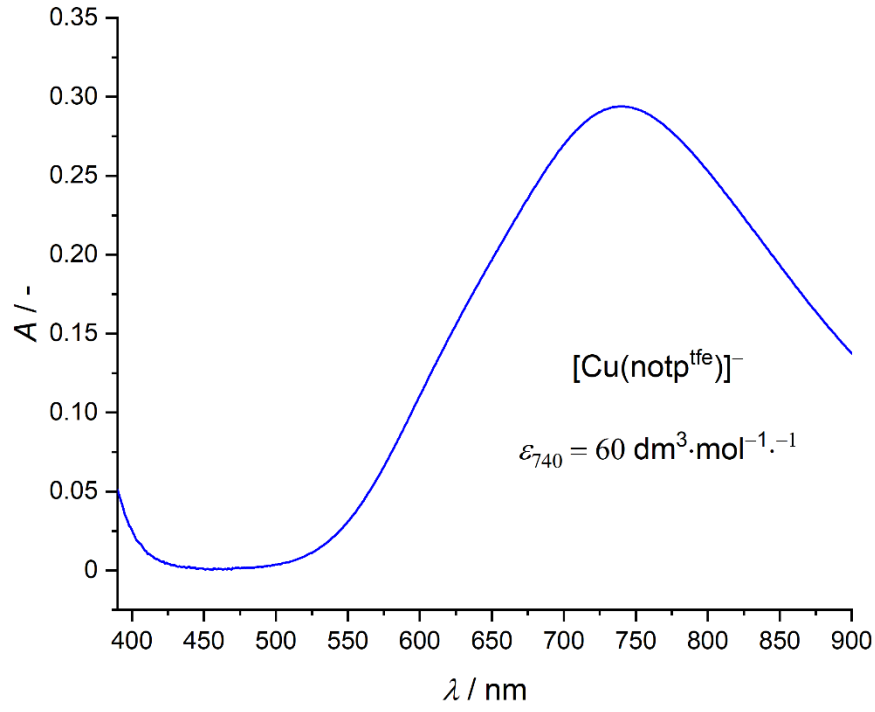

Figure S19. UV-Vis spectrum of $[Cu^{II}(notp^{tfe})]^-$ (HEPES, pH 7.4).

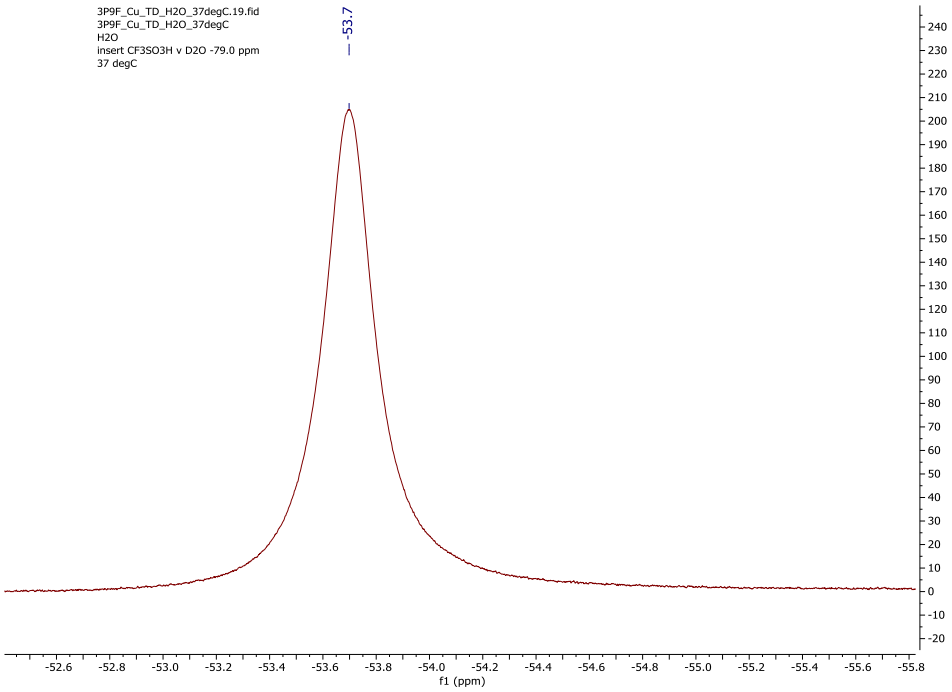

Figure S20. ^{19}F NMR spectra of $[Cu^{II}(notp^{tfe})]^-$ (D_2O, pD 7.4, 37 °C, 565 MHz).

$[Zn^{II}(notp^{tfe})]^-$

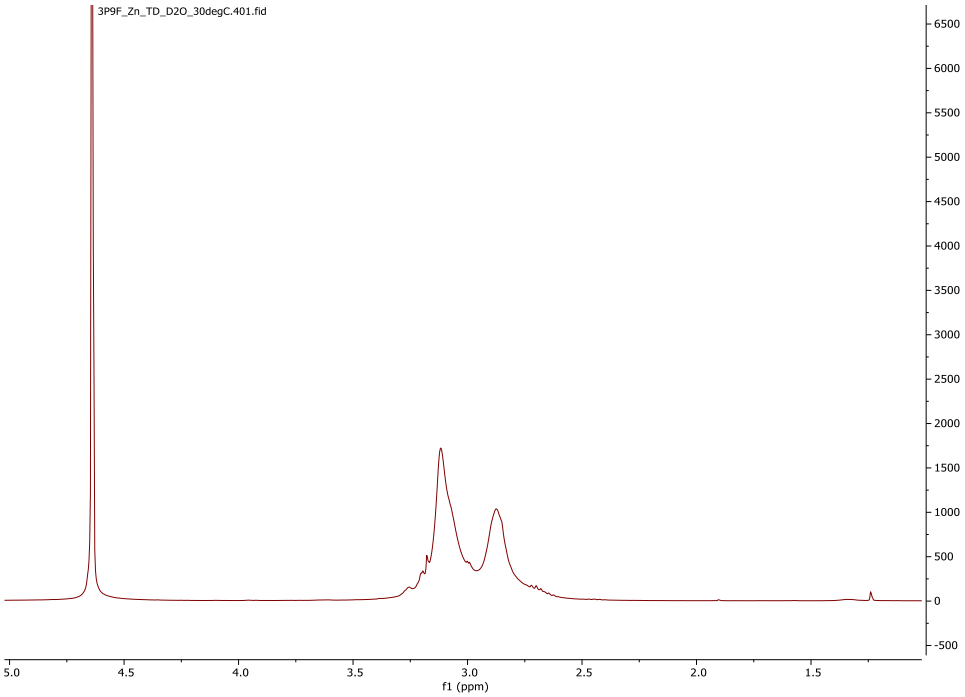

Figure S21. ^1H NMR spectra of $[Zn^{II}(notp^{tfe})]^-$ (D_2O, pD 7.4, 37 °C, 600 MHz).

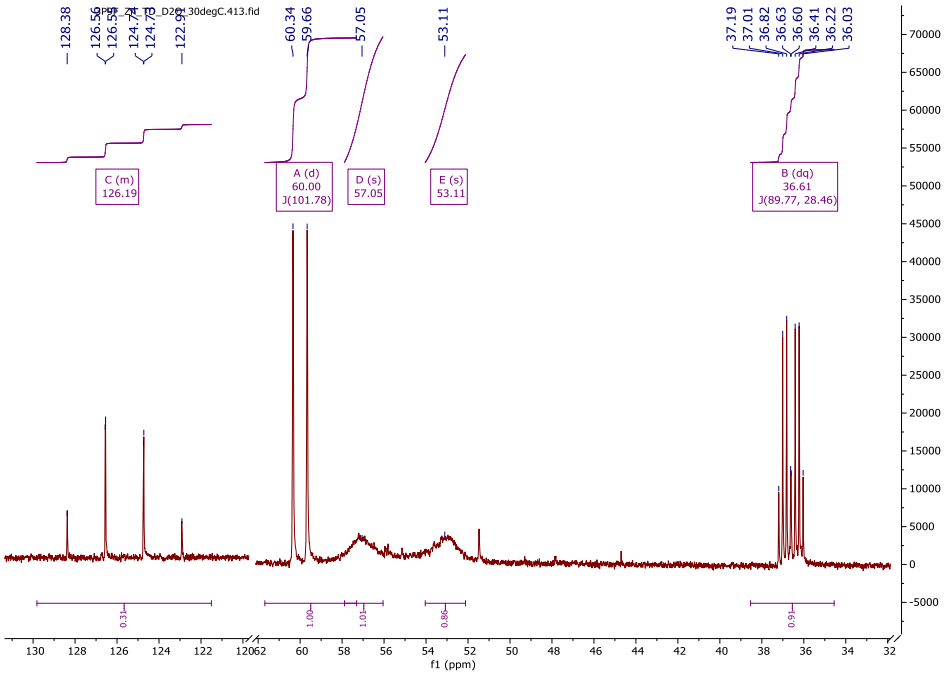

Figure S22. $^{13}C\{^{1}H\}$ NMR spectra of $[Zn^{II}(notp^{tfe})]^{-}$ (D_2O, pD 7.4, 37 °C, 151 MHz).

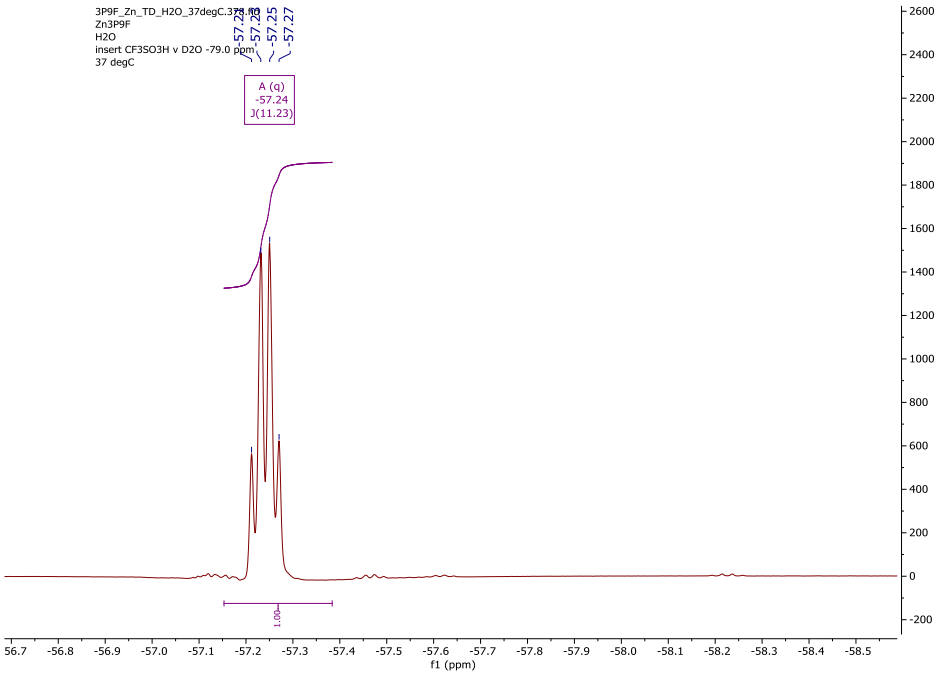

Figure S23. ^{19}F NMR spectra of $[Zn^{II}(notp^{tfe})]^{-}$ (D_2O, pD 7.4, 37 °C, 565 MHz).

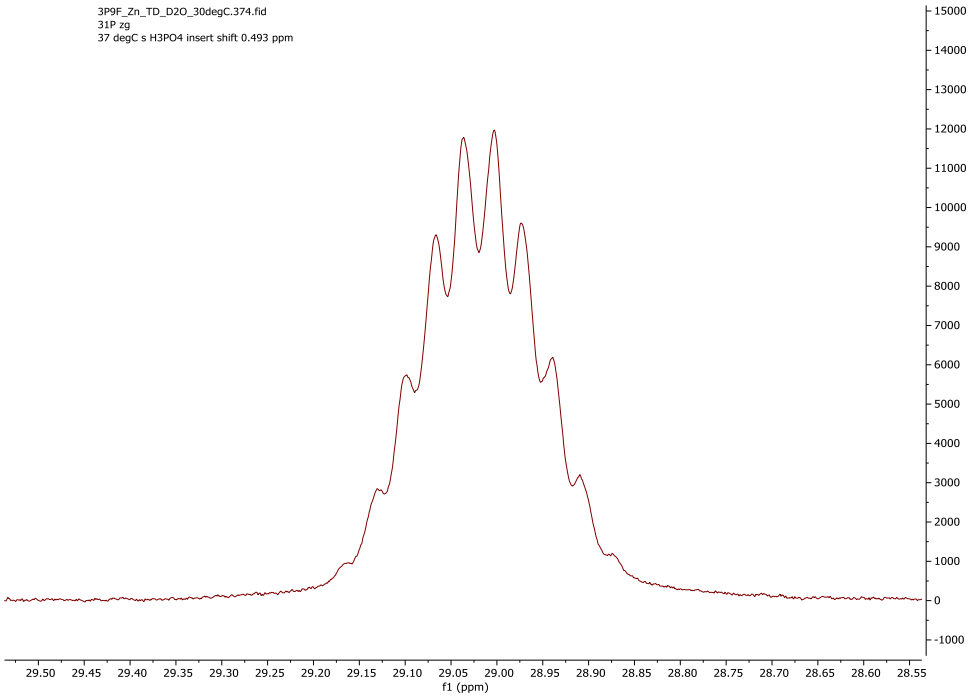

Figure S24. ^{31}P NMR spectra of $[Zn^{II}(notp^{tfe})]^-$ (D_2O, pD 7.4, 37 °C, 262 MHz).

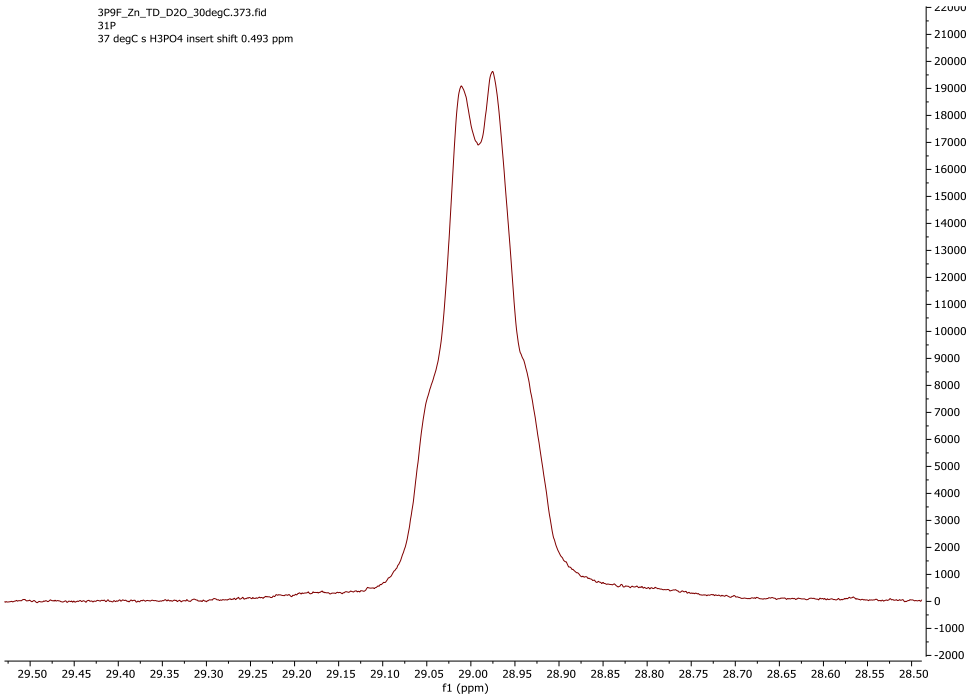

Figure S25. ^{31}P{^{1}H} NMR spectra of $[Zn^{II}(notp^{tfe})]^-$ (D_2O, pD 7.4, 37 °C, 262 MHz).

Distribution diagrams of H_3notp^{tfe} and the M^{2+}–H_3notp^{tfe} systems

Table S3. Logarithms of overall protonation constants ($\log\beta_h$) and stability constants ($\log\beta_{hml}$) of H_3notp^{tfe} and its studied metal complexes. The overall protonation constants are defined as $\beta_h = [H_hL] / ([H]^h \cdot [L])$, the overall stability constants are defined by $\beta_{hml} = [M_mH_hL_l] / ([M]^m \cdot [H]^h \cdot [L]^l)$. Charges of the species are omitted for clarity; "L" means fully deprotonated form of the ligand, $(notp^{tfe})^{3-}$.

Ion	*h*			log(β_h)
H^+	1			10.23(1)
	2			13.10(1)

	h	*l*	*m*	log(β_{hml})
Mg^{2+}	0	1	1	5.08(5)
	−1	1	1	−6.63(5)
Ca^{2+}	0	1	1	3.83(1)
	−1	1	1	−9.03(3)
Mn^{2+}	0	1	1	10.61(2)
	−1	1	1	0.44(4)
Co^{2+}	0	1	1	13.04(3)
Ni^{2+}	0	1	1	13.18(3)
Cu^{2+}	0	1	1	13.50(3)
	−1	1	1	1.93(4)
Zn^{2+}	0	1	1	13.40(4)
	−1	1	1	1.14(6)

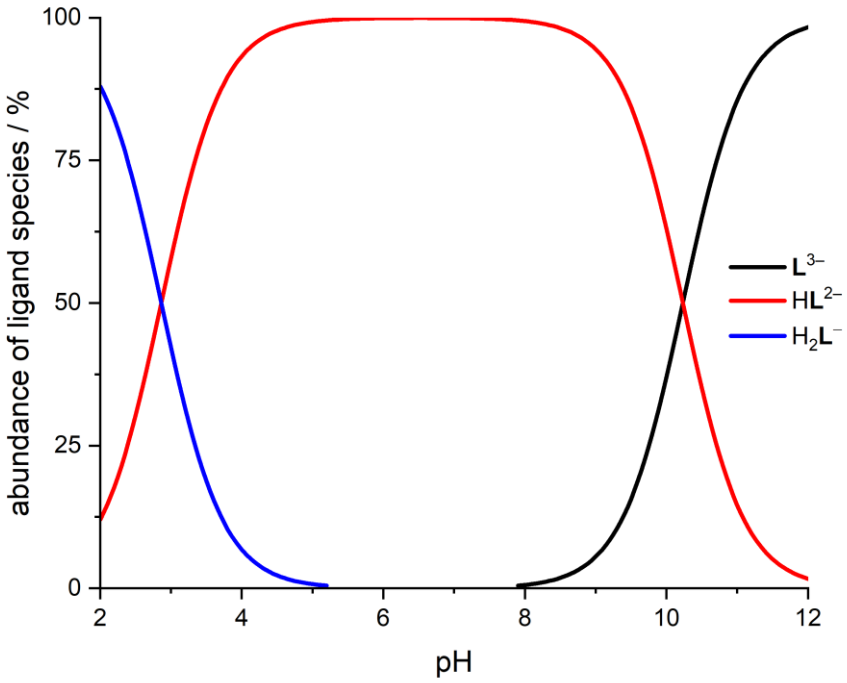

Figure S26. Distribution diagram of H_3notp^{tfe} (= H_3**L**). *c*(H_3notp^{tfe}) = 0.004 M.

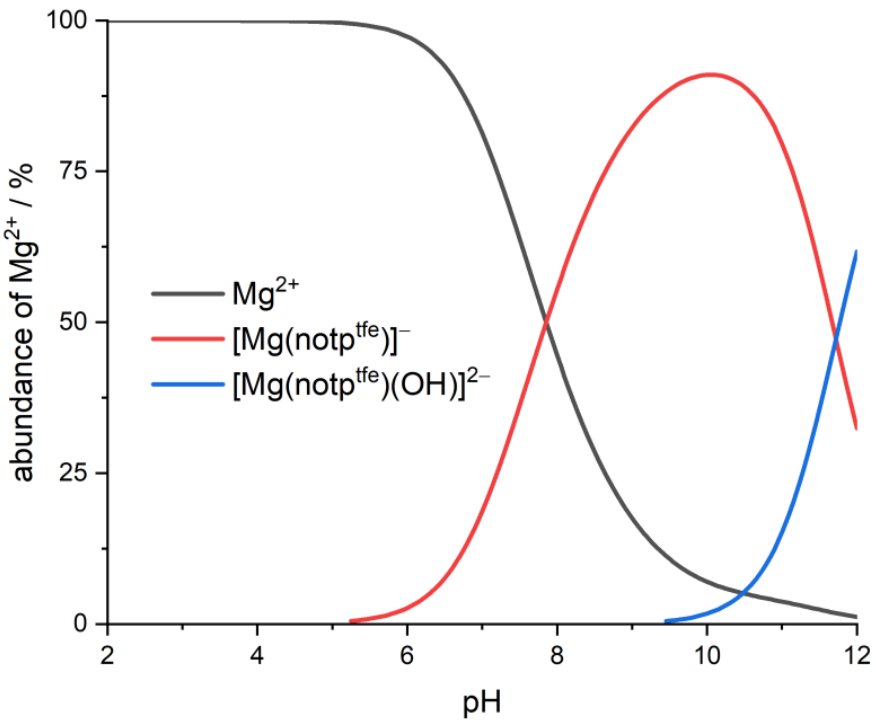

Figure S27. Distribution diagram of the Mg^{2+}–H_3notp^{tfe} system; $c(Mg^{2+}) = c(H_3notp^{tfe})$ = 0.004 M.

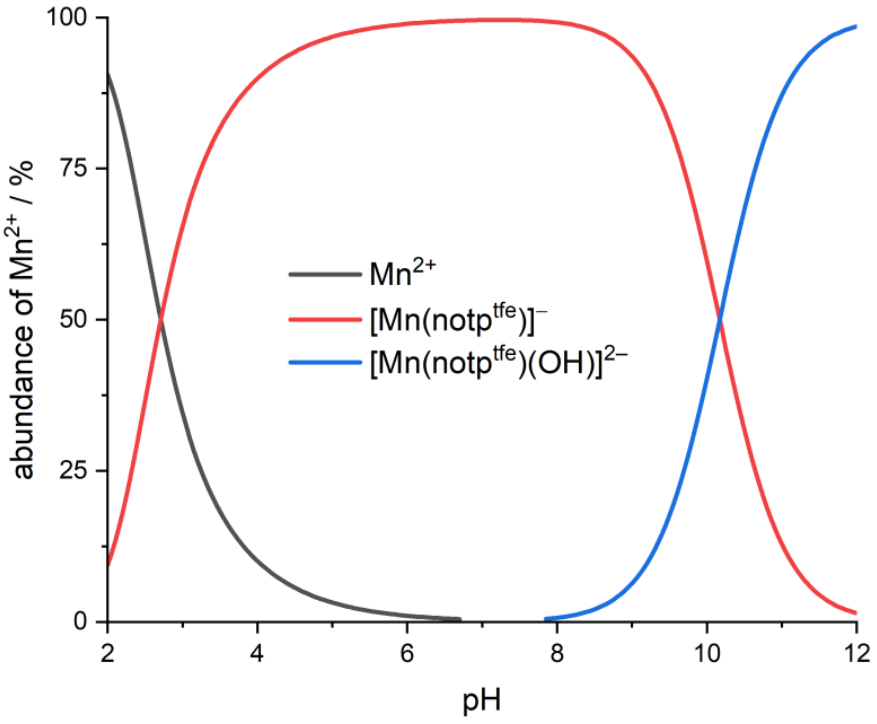

Figure S28. Distribution diagram of the Mn^{2+}–H_3notp^{tfe} system; $c(Mn^{2+}) = c(H_3notp^{tfe})$ = 0.004 M.

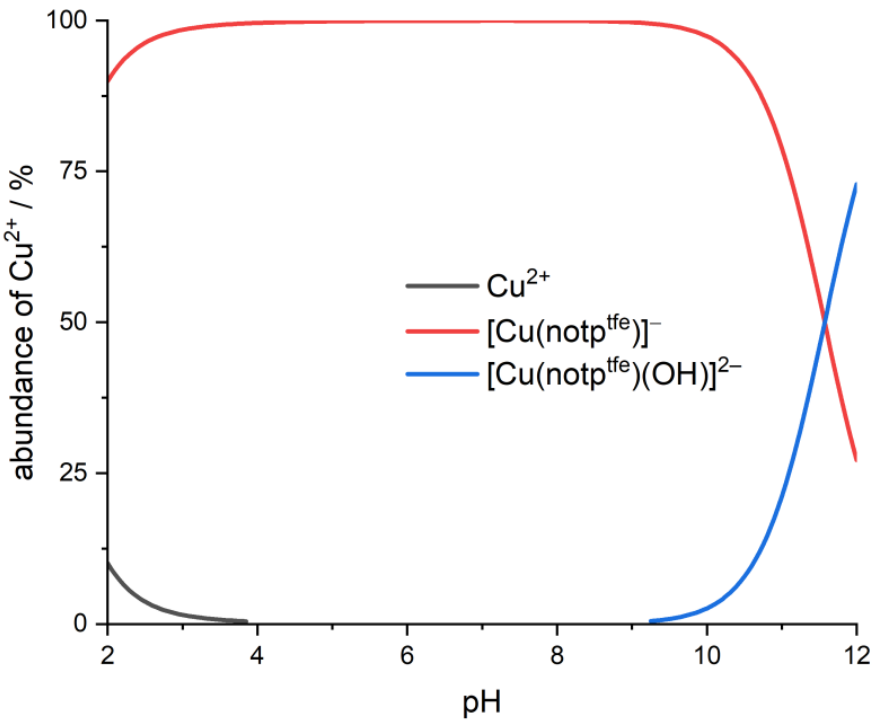

Figure S29. Distribution diagram of the Cu^{2+}–H_3notp^{tfe} system; $c(Cu^{2+}) = c(H_3notp^{tfe})$ = 0.004 M.

Spectro-electrochemical measurements

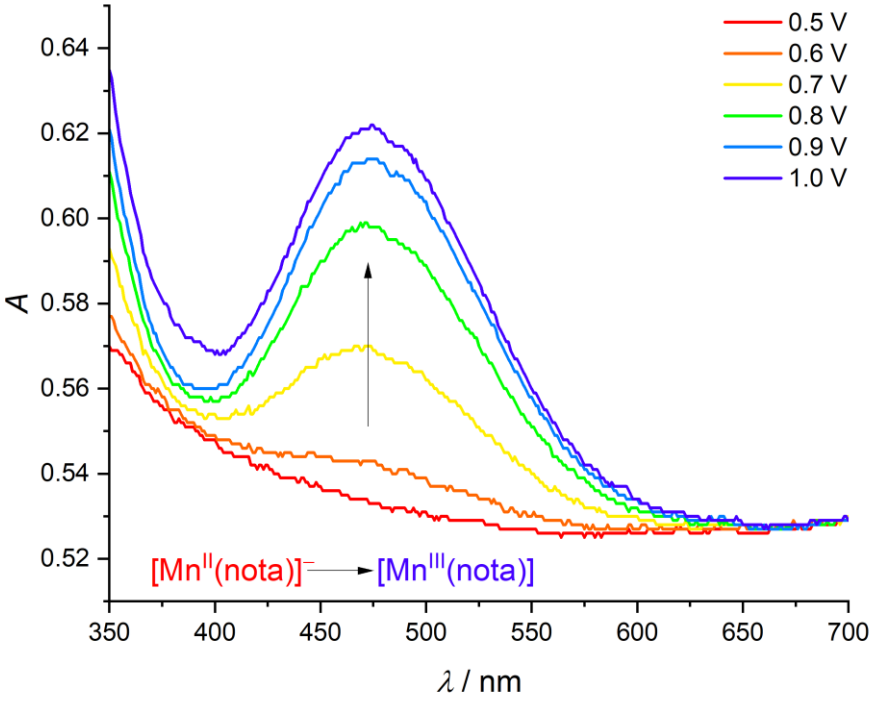

Figure S30. Change of absorption spectra of $[Mn^{II}(nota)]^-$ with increase of oxidation potential during spectro-electrochemical measurements due to formation of $[Mn^{III}(nota)]$.

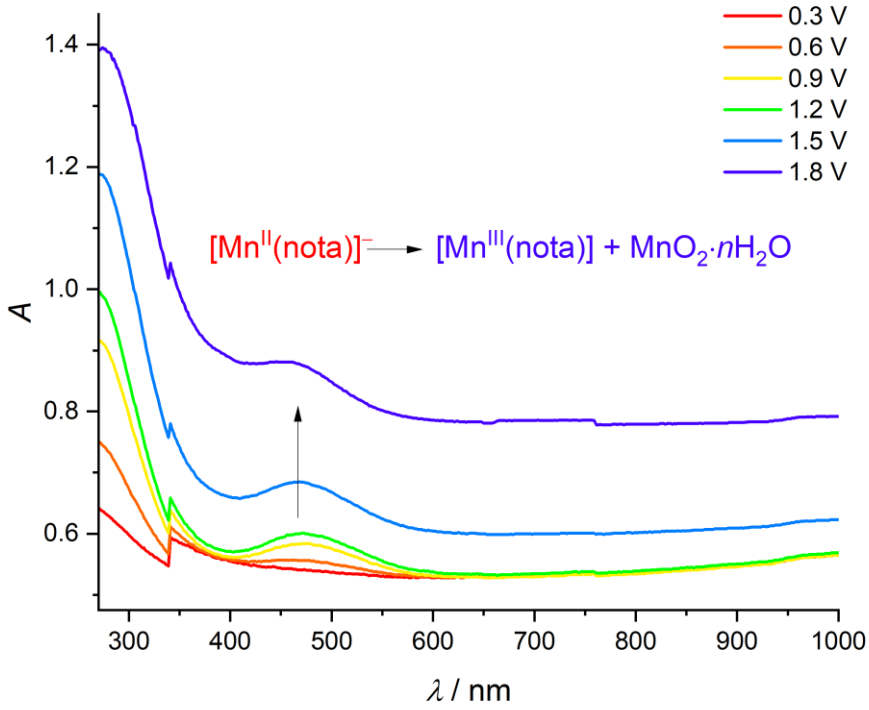

Figure S31. Change of absorption spectra of $[Mn^{II}(nota)]^-$ with increase of oxidation potential during spectro-electrochemical measurements due to formation of $[Mn^{III}(nota)]$ and colloidal $Mn^{IV}O_2$.

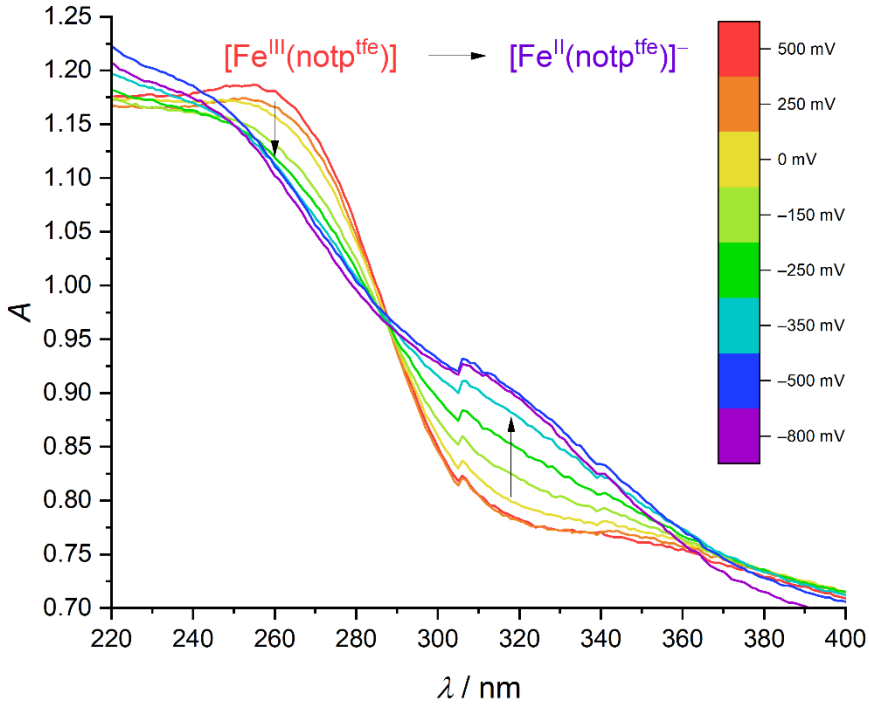

Figure S32. Change of absorption spectra of $[Fe^{III}(notp^{tfe})]$ with decrease of potential during spectro-electrochemical measurements due to formation of $[Fe^{II}(notp^{tfe})]^-$.

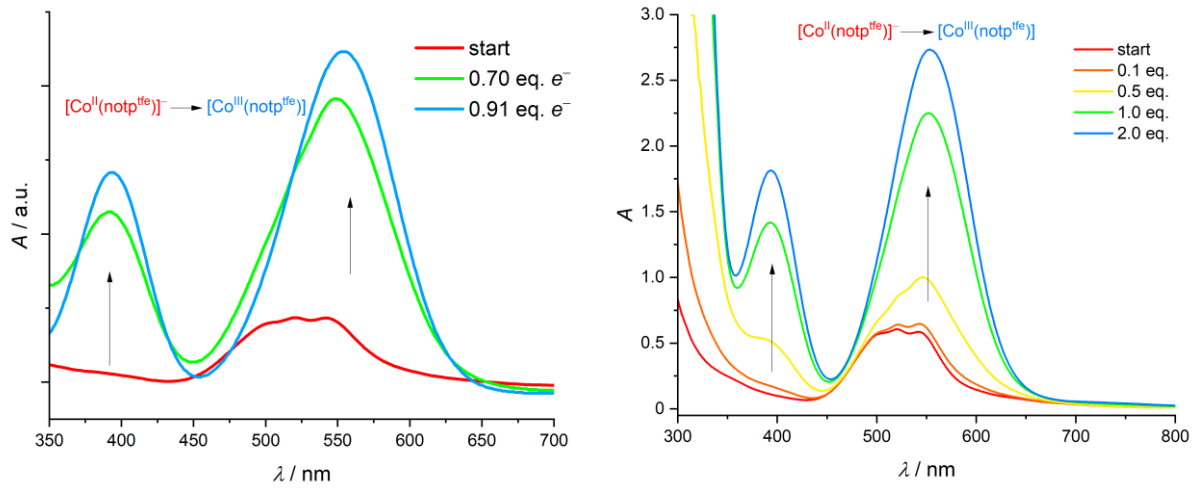

Figure S33. Change of absorption spectra of $[Co^{II}(notp^{tfe})]^-$ during oxidation to $[Co^{III}(notp^{tfe})]$ by electrosynthesis (left) or by oxidation with $K_2S_2O_8$ (right).

Single-crystal X-ray diffraction study

The selected crystals were mounted on a glass fibre in a random orientation and the diffraction data were collected by Bruker D8 VENTURE Duo diffractometer with a micro-focus sealed tube using Cu-K_α radiation (λ 1.54178 Å) at 120 K {ammonium (2,2,2-trifluoroethyl)phosphinate, $Na_3[Co(\mathbf{L})]_2Br{\cdot}3Me_2CO$} or Mo-$K_\alpha$ radiation (λ 0.71073 Å) at 180 K {$(NH_4)[Cu(\mathbf{L})]{\cdot}3.5H_2O$}, 150 K [1-adamantylammonium (2,2,2-trifluoroethyl)phosphinate] or at 120 K (all other structures). Data were analysed using the SAINT software package (Bruker AXS Inc., 2015–2019). Data were corrected for absorption effects using the multi-scan method (SADABS).[1] All structures were solved by direct methods (SHELXT2014)[2] and refined using full-matrix least-squares techniques (SHELXL2017).[3]

In general, all non-hydrogen atoms were refined anisotropically. The hydrogen atoms were localised in the electron density map; however, those bound to the carbon atoms were placed in theoretical positions using $U_{eq}(H) = 1.2\ U_{eq}(C)$ to keep the number of parameters low and only hydrogen atoms bound to heteroatoms (N, O, P) were fully refined. Some hydrogen atoms belonging to the O–H or N–H groups were fixed in original or theoretical positions, if their full refinement led to unrealistically short or long bonding distances. Details on the structure refinements are given below. For overview of experimental crystallographic data see Table S4, selected geometric parameters are listed in Tables 4 and S5.

---

[1] L. Krause, R. Herbst-Irmer, G. M. Sheldrick and D. Stalke, *J. Appl. Cryst.*, 2015, **48**, 3–10.

[2] (*a*) G. M. Sheldrick, *SHELXT2014/5. Program for Crystal Structure Solution from Diffraction Data*, University of Göttingen, Göttingen, 2014; (*b*) G. M. Sheldrick, *Acta Crystallogr. Sect. A.*, 2008, **A64**, 112–122.

[3] (*a*) C. B. Hübschle, G. M. Sheldrick and B. Dittrich, *ShelXle: a Qt graphical user interface for SHELXL*, University of Göttingen, Göttingen, 2014. (*b*) C. B. Hübschle, G. M. Sheldrick and B. Dittrich, *J. Appl. Cryst.*, 2011, **44**, 1281–1284. (*c*) G. M. Sheldrick, *Acta Crystallogr. Sect. C*, 2015, **C71**, 3–8. (*d*) G. M. Sheldrick, *SHELXL-2017/1. Program for Crystal Structure Refinement from Diffraction Data*, University of Göttingen, Göttingen, 2017.

Table S4. Experimental crystallographic data for reported crystal structures [**L** = $(notp^{tfe})^{3-}$].

Compound	2,2,2-Trifluoroethyl--tosylate	Ammonium (2,2,2-trifluoroethyl)phosphinate	1-Adamantylammonium (2,2,2-trifluoroethyl)phosphinate	$(NH_4)_3[Mn(\mathbf{L})]Cl_2 \cdot 3H_2O$	$[Mn(H_2O)_6][Mn(\mathbf{L})]_2 \cdot 18H_2O$	$(NH_4)[Co(\mathbf{L})] \cdot 3.5H_2O$
Formula	$C_9H_9F_3O_3S$	$C_2H_7F_3NO_2P$	$C_{12}H_{21}F_3NO_2P$	$C_{15}H_{42}Cl_2F_9MnN_6O_9P_3$	$C_{30}H_{96}F_{18}Mn_3N_6O_{36}P_6$	$C_{15}H_{35}CoF_9N_4O_{9.5}P_3$
M	254.22	165.06	299.27	840.29	1809.76	746.31
Crystal system	monoclinic	orthorhombic	monoclinic	monoclinic	trigonal	monoclinic
Space group	$P2_1/c$	P b c a	$P2_1/c$	$P2_1/n$	$R\bar{3}$: H	$C2/c$
a / Å	8.2859(4)	7.3490(4)	12.9012(4)	16.6902(5)	17.3178(3)	25.658(2)
b / Å	11.5440(6)	11.7365(6)	6.5370(2)	11.6001(4)	17.3178(3)	9.3786(7)
c / Å	11.0029(5)	15.2447(8)	17.6777(6)	17.4365(6)	21.8650(7)	24.137(2)
α / °	90	90	90	90	90	90
β / °	93.944(2)	90	110.443(1)	92.070(1)	90	100.726(3)
γ / °	90	90	90	90	120	90
U / Å^3	1049.96(9)	1314.88(12)	1396.96(8)	3373.64(19)	5678.9(3)	5706.6(8)
Z	4	8	4	4	3	8
Unique refl.	2412	1287	3214	7735	2890	6587
Obsd. refl.	2356	1283	2816	7231	2770	6208
$R(I>2\sigma(I))$; *R'*	0.0281; 0.0287	0.0259; 0.0259	0.0315; 0.0379	0.0288; 0.0308	0.0340; 0.0358	0.0440; 0.0463
$wR(I>2\sigma(I))$; *wR'*	0.0743; 0.0748	0.0759; 0.0759	0.0834; 0.0873	0.0808; 0.0823	0.0970; 0.1100	0.1024; 0.1035
CCDC ref. no.	2327151	2327148	2327149	2327152	2327147	2327154

Table S4. Experimental crystallographic data for reported crystal structures – continuation.

Compound	$[Co(H_2O)_6][Co(\mathbf{L})]_2 \cdot 14.25H_2O \cdot 0.75MeOH$	$Na_3[Co(\mathbf{L})]_2Br \cdot 3Me_2CO$	$(NH_4)[Cu(\mathbf{L})] \cdot 3.5H_2O$	$(NH_4)_2[Cu(\mathbf{L})]Cl \cdot 3H_2O$	$[Mg(H_2O)_6][Ni(\mathbf{L})]_2 \cdot 12H_2O$	$[ZnCl(H_2O)_3][Zn(\mathbf{L})] \cdot 2H_2O$
Formula	$C_{30.75}H_{91.5}Co_3F_{18}N_6O_{33}P_6$	$C_{39}H_{66}BrCo_2F_{18}N_6Na_3O_{15}P_6$	$C_{15}H_{35}CuF_9N_4O_{9.5}P_3$	$C_{15}H_{38}ClCuF_9N_5O_9P_3$	$C_{30}H_{84}F_{18}MgN_6Ni_2O_{30}P_6$	$C_{15}H_{34}ClF_9N_3O_{11}P_3Zn_2$
M	1778.20	1653.53	750.92	795.40	1678.58	862.55
Crystal system	trigonal	monoclinic	monoclinic	triclinic	trigonal	cubic
Space group	*R*−3: H	$P2_1/c$	*C*2/*c*	*P*−1	*R*−3: H	$P2_13$
a / Å	34.3841(8)	13.7602(6)	25.578(1)	8.3574(2)	17.5880(4)	14.7089(2)
b / Å	34.3841(8)	14.0687(6)	9.4016(3)	10.8556(3)	17.5880(4)	14.7089(2)
c / Å	40.961(2)	32.878(1)	24.4262(8)	17.8608(4)	18.4148(6)	14.7089(2)
α / °	90	90	90	99.815(1)	90	90
β / °	90	93.802(2)	101.072(1)	92.158(1)	90	90
γ / °	120	90	90	110.264(1)	120	90
U / Å^3	41939(2)	6350.7(5)	5764.4(3)	1489.65(6)	4933.2(3)	3182.30(13)
Z	24	4	8	2	3	4
Unique refl.	21382	15764	6568	6824	2516	2426
Obsd. refl.	15240	13905	6169	6055	2478	2380
$R(I>2\sigma(I))$; *R'*	0.0362; 0.0601	0.0945; 0.1020	0.0272; 0.0291	0.0315; 0.0365	0.0197; 0.0200	0.0266; 0.0274
$wR(I>2\sigma(I))$; *wR'*	0.0877; 0.1024	0.2563; 0.2617	0.0739; 0.0753	0.0814; 0.0850	0.0498; 0.0500	0.0673; 0.0678
CCDC ref. no.	2327158	2327157	2327153	2327156	2327155	2327150

Table S5. Selected geometric parameters found in the crystal structures of studied complexes [$\mathbf{L}^{3-}$ = $(notp^{tfe})^{3-}$].

	$(NH_4)_3[Mn(\mathbf{L})]Cl_2$ ·$3H_2O$	$[Mn(H_2O)_6][Mn(\mathbf{L})]_2$ ·$18H_2O$	$(NH_4)[Co(\mathbf{L})]$ ·$3.5H_2O$	$[Co(H_2O)_6][Co(\mathbf{L})]_2$ ·$14.25H_2O$·0.75MeOH				$Na_3[Co(\mathbf{L})]_2Br$ ·$3Me_2CO$		$(NH_4)[Cu(\mathbf{L})]$ ·$3.5H_2O$	$(NH_4)_2[Cu(\mathbf{L})]Cl$ ·$3H_2O$	$[Mg(H_2O)_6][Ni(\mathbf{L})]_2$ ·$12H_2O$	$[ZnCl(H_2O)_3][Zn(\mathbf{L})]$ ·$2H_2O$
Geometry	TTA	TTA[a]	OC	TTA	TTA	TTA[a]	TTA[a]	TTA	TTA	OC	square pyramidal	OC[a]	OC[a]
	Δδ-*SSS*	Δδ-*SSS*	Δλ-*SSS*	Λλ-*RRR*	Δδ-*SSS*	Λλ-*RRR*	Δδ-*SSS*	Λλ-*SSS*	Λλ-*SSS*	Λδ-*RRR*	ΔΛ-λλλ-*SR*	Λδ-*RRR*	Λδ-*RRR*
							Angles (°)						
N1–M–N4	75.42(5)	76.49(7)	83.25(9)	81.23(7)	80.75(6)	80.57(7)	81.01(7)	82.1(3)	82.8(3)	84.91(5)	85.89(7)	84.63(4)	81.7(1)
N1–M–N7	76.69(5)	76.49(7)	81.94(9)	81.14(6)	81.50(6)	80.57(7)	81.01(7)	81.7(3)	82.0(3)	81.46(5)	84.09(7)	84.63(4)	81.7(1)
N1–M–O11	80.59(5)	80.15(6)	85.48(8)	83.01(6)	83.04(6)	83.13(6)	83.18(6)	82.5(3)	81.4(3)	85.50(5)	89.93(7)	85.86(3)	84.3(1)
N1–M–O21	137.36(5)	150.05(7)	95.59(9)	157.10(6)	157.32(6)	155.79(6)	160.12(7)	158.9(3)	158.6(3)	98.16(5)	161.44(7)	96.67(3)	102.7(1)
N1–M–O31	129.19(5)	115.86(7)	165.80(9)	112.58(6)	112.68(6)	114.24(6)	108.34(7)	107.5(3)	107.1(3)	163.46(5)	–	170.24(3)	164.6(1)
N4–M–N7	75.46(5)	76.49(7)	82.23(9)	81.37(6)	81.42(6)	80.57(7)	81.01(7)	82.0(3)	82.3(3)	84.32(5)	84.33(6)	84.63(4)	81.7(1)
N4–M–O11	129.05(5)	115.86(7)	167.97(8)	108.81(6)	109.11(6)	114.24(6)	108.34(7)	110.1(3)	110.5(3)	169.93(5)	172.28(6)	170.24(3)	164.6(1)
N4–M–O21	80.02(5)	80.15(6)	83.32(8)	82.38(6)	81.75(6)	83.13(6)	83.18(6)	84.3(3)	82.3(3)	86.39(5)	88.27(6)	85.86(3)	84.33(1)
N4–M–O31	141.13(5)	150.05(7)	99.16(9)	156.51(6)	156.94(6)	155.79(6)	160.12(7)	159.7(3)	160.2(3)	98.38(5)	–	96.67(3)	102.7(1)
N7–M–O11	140.28(5)	150.05(7)	100.36(8)	159.59(6)	159.60(6)	155.79(6)	160.12(7)	158.6(3)	157.5(3)	97.26(5)	101.71(6)	96.67(3)	102.7(1)
N7–M–O21	129.47(5)	115.86(7)	165.53(9)	112.03(6)	109.97(6)	114.24(6)	108.34(7)	112.2(3)	111.1(3)	170.69(5)	112.86(6)	170.24(3)	164.6(1)
N7–M–O31	81.78(5)	80.15(6)	84.51(9)	82.18(6)	82.21(6)	83.13(6)	83.18(6)	81.8(3)	82.1(3)	82.74(5)	–	85.86(3)	84.3(1)
O11–M–O21	88.80(5)	93.65(6)	93.63(8)	87.26(6)	89.19(6)	87.42(6)	90.47(6)	87.2(3)	89.4(3)	91.97(4)	93.71(6)	93.07(3)	92.5(1)
O11–M–O31	88.05(5)	93.65(6)	92.80(7)	92.18(6)	91.60(6)	87.42(6)	90.47(6)	89.2(3)	88.3(3)	91.68(4)	–	93.07(3)	92.5(1)
O21–M–O31	91.15(5)	93.65(6)	98.59(9)	88.39(6)	88.73(6)	87.42(6)	90.47(6)	90.6(3)	91.9(3)	98.22(5)	–	93.07(3)	92.5(1)
NQ···Co1···OQ[b]	178.03(2)	180	179.50(4)	177.71(2)	177.56(2)	180	180	178.0(1)	178.0(1)	174.12(2)	–	180	180

[a] Complex molecule possess trigonal symmetry; F1 = F4 = F7, F2 = F5 =F8, F3 = F6 = F9. [b] NQ and OQ are centroids of the N_3- and O_3- planes, respectively.

In all crystal structures of organic intermediates, one formula unit forms the structurally independent unit. In the crystal structure of 2,2,2-trifluoroethyl-tosylate the methyl group was best refined staggered in two positions with relative occupancy 50:50%. In the crystal structures of ammonium 2,2,2-trifluoroethylphosphinate and 1-adamantylammonium 2,2,2-trifluoroethylphosphinate, all hydrogen atoms attached to nitrogen and phosphorus atoms were fully refined.

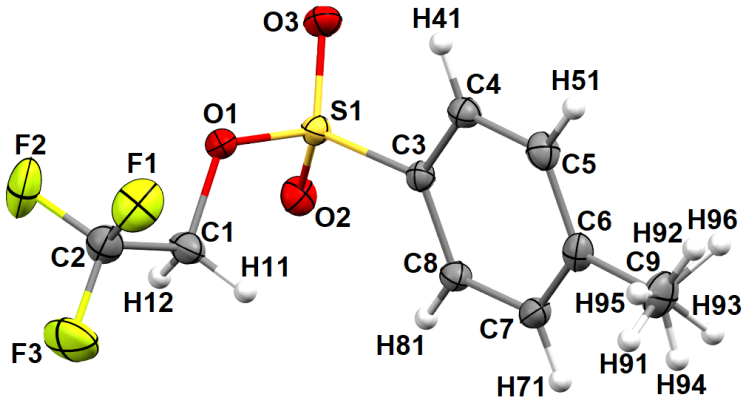

Figure S34. Molecular structure of 2,2,2-trifluoroethyl-tosylate found in its crystal structure. A disorder of the methyl group staggered in two positions is shown.

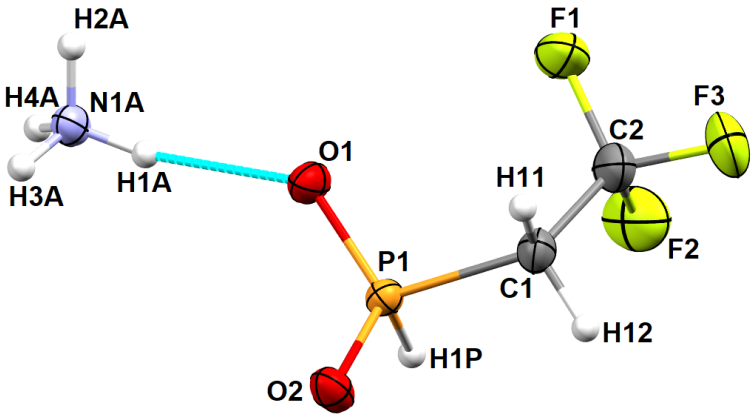

Figure S35. Independent unit found in the crystal structure of ammonium 2,2,2-trifluoroethylphosphinate. The shortest intermolecular hydrogen bond is shown in turquoise [*d*(N1A···O1) = 2.76 Å].

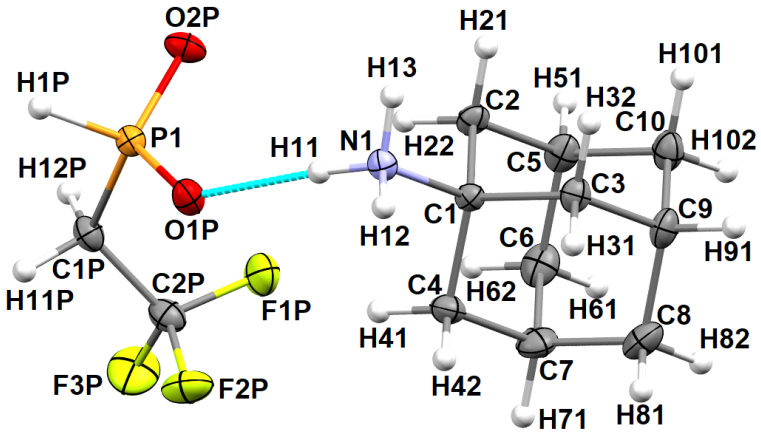

Figure S36. Independent unit found in the crystal structure of 1-adamantylammonium 2,2,2-trifluoroethylphosphinate. The shortest intermolecular hydrogen bond is shown in turquoise [*d*(N1···O1P) = 2.74 Å].

In the crystal structure of $(NH_4)_3[Mn(\mathbf{L})]Cl_2{\cdot}3H_2O$, one formula unit forms the structurally independent unit and no disorder was found. Two hydrogen atoms bound in one of ammonium cations were fixed in reliable distance from the nitrogen atom as their full refinement led to unrealistically long bonds but all other hydrogen atoms of ammonium cations and water molecules were fully refined.

In the crystal structure of $[Mn(H_2O)_6][Mn(\mathbf{L})]_2{\cdot}18H_2O$, one-sixth of the formula unit forms the structurally independent unit due to the symmetry of the space group *R*−3; the complex species $[Mn(\mathbf{L})]^-$ possess trigonal symmetry. Two hydrogen atoms of water molecules of crystallization were fixed in reliable distance from the oxygen atom as their full refinement led to unrealistically long bonds, but all other hydrogen atoms of water molecules were fully refined.

The crystal structures of $(NH_4)[Co(\mathbf{L})]{\cdot}3.5H_2O$ and $(NH_4)[Cu(\mathbf{L})]{\cdot}3.5H_2O$ are isostructural; one formula unit forms the structurally independent unit. One pendant arm was refined disordered in two positions, sharing the carbon atom of the N–C–P fragment and the coordinated oxygen atom. Relative occupancies were 68:31% and 67:33%, respectively (Figures S37 and S41). Also one of water molecules of crystallization was best refined disordered in two positions with 86:14 and 67:33%, respectively.

In the crystal structure of $[Co(H_2O)_6][Co(\mathbf{L})]_2{\cdot}14.25H_2O{\cdot}0.75MeOH$, two complexes $[Co(\mathbf{L})]^-$ connected head-to-head through the aqua ion $[Co(H_2O)_6]^{2+}$ were found (Figure S38) and one of them has crystallographic trigonal symmetry; thus, one and one-third of the formula unit form the structurally independent part. Hydrogen atoms belonging to the water molecules of crystallization were fixed in original positions. The oxygen atoms of methanol of crystallization was refined disordered in two positions with relative occupancy 55:45% sharing the carbon atom.

In the crystal structure of $Na_3[Co(\mathbf{L})]_2Br{\cdot}3Me_2CO$ (Figure S39), one formula unit forms the structurally independent unit. One of molecules of acetone disordered over two positions was found with relative

occupancy 60:40%, with overlap of the carbonyl carbon atom. There are relatively large difference maxima very close to position of the bromide ion; however, this disorder cannot be reliably modelled. Data quality of this crystal was relatively low, as reflected by a high value of the *R*-factor.

In the crystal structure of $[Mg(H_2O)_6][Ni(\mathbf{L})]_2 \cdot 12H_2O$, one-sixth of the formula unit forms the structurally independent unit due to the symmetry of the space group *R*−3; the $[Ni(\mathbf{L})]^-$ complex species possess trigonal symmetry (Figure S40). No disorder was found and all hydrogen atoms of water molecules were fully refined.

In the crystal structure of $(NH_4)_2[Cu(\mathbf{L})]Cl \cdot 3H_2O$, one formula unit forms the structurally independent unit. Large electron maxima around chloride ion in preliminary solution were finally interpreted as disordered chloride in total in three close positions with 0.82, 0.10 and 0.08% occupancy. Two hydrogen atoms of one ammonium cation and one hydrogen atom of one of water molecules of crystallization were fixed at reliable distance from the corresponding nitrogen or oxygen atom, respectively, as their full refinement led to unrealistically long/short bond distances.

In the crystal structure of $[ZnCl(H_2O)_3][Zn(\mathbf{L})] \cdot 2H_2O$, one-third of the formula unit forms the structurally independent unit due to trigonal symmetry of the $[ZnCl(H_2O)_3]^+$ and $[Zn(\mathbf{L})]^-$ species (Figure S43). Hydrogen atoms of water molecules were fixed in original positions as their full refinement led to unreasonable bond distances and thermal factors.

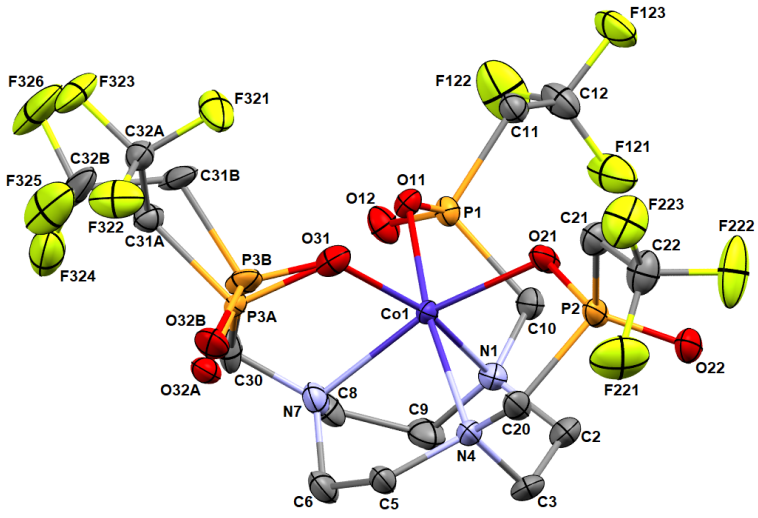

Figure S37. Molecular structure of $[Co(notp^{tfe})]^-$ anion with the Δλ-*SSS* OC geometry found in the crystal structure of $(NH_4)[Co(notp^{tfe})] \cdot 3.5H_2O$. Disorder of the pendant arm (attached to nitrogen atom N7) is shown. Hydrogen atoms are omitted for clarity.

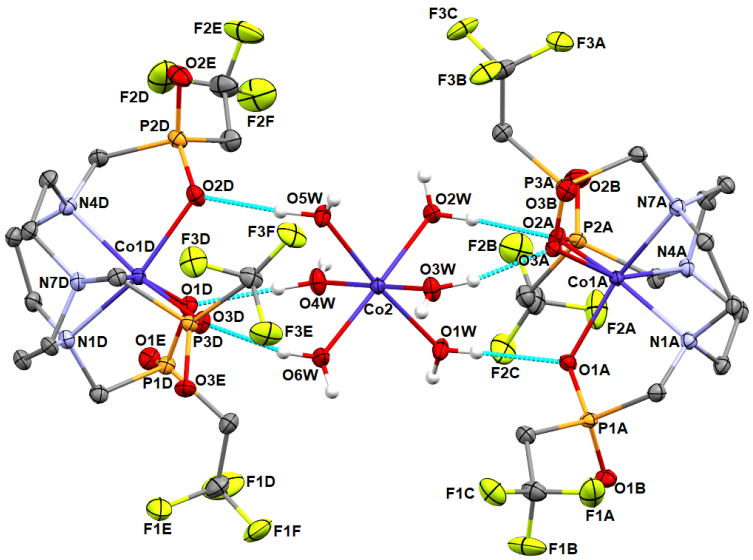

Figure S38. Molecular structure of one of $[Co(H_2O)_6][Co(notp^{tfe})]_2$ structurally independent fragments found in the crystal structure of $[Co(H_2O)_6][Co(notp^{tfe})]_2 \cdot 14.25H_2O \cdot 0.75MeOH$. Intermolecular hydrogen bonds connecting two $[Co(notp^{tfe})]^-$ anions through hydrogen bonds to the central $[Co(H_2O)_6]^{2+}$ cation are shown in turquoise. Individual $[Co(notp^{tfe})]^-$ species adopt the Δδ-*SSS* / Λλ-*RRR* TTA geometries. Carbon-bound hydrogen atoms and labelling of carbon and hydrogen atoms are omitted for clarity.

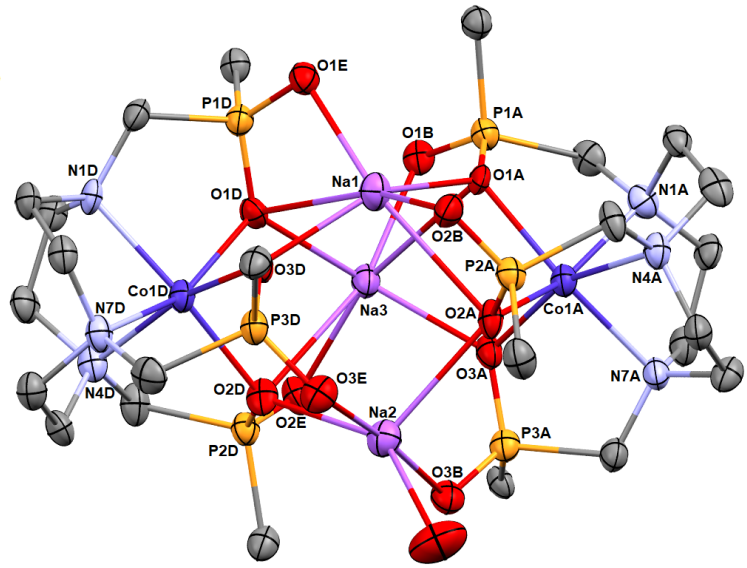

Figure S39. Molecular structure of $Na_3[Co(notp^{tfe})]_2^+$ found in the crystal structure of $Na_3[Co(notp^{tfe})]_2Br \cdot 3Me_2CO$. Both $[Co(notp^{tfe})]^-$ complexes in the shown species adopt the Λλ-*SSS* TTA geometry; the Δδ-*RRR* TTA species are present in the crystal structure due to centrosymmetry of the space group ($P2_1/c$). Terminal trifluoromethyl groups, hydrogen atoms and labelling of carbon atoms are omitted for clarity.

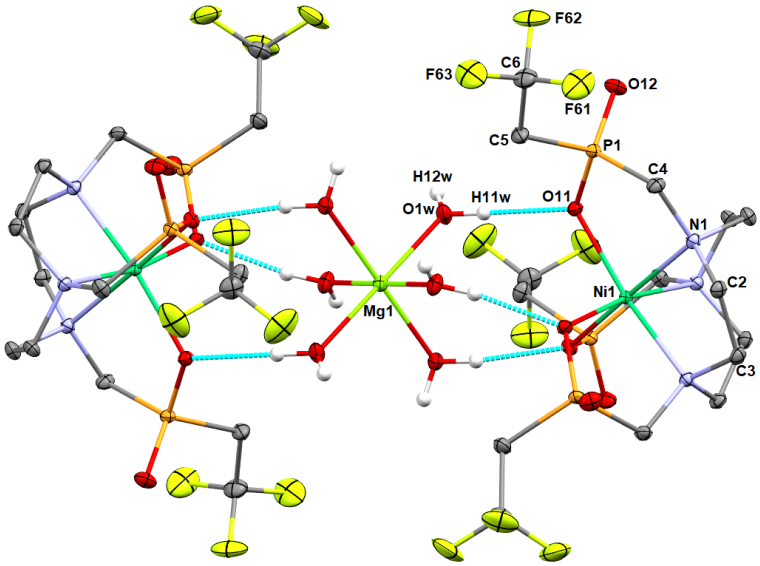

Figure S40. Molecular structure of $[Mg(H_2O)_6][Ni(notp^{tfe})]_2$ fragment found in the crystal structure of $[Mg(H_2O)_6][Ni(notp^{tfe})]_2 \cdot 12H_2O$. Intermolecular hydrogen bonds connecting two $[Ni(notp^{tfe})]^-$ anions through hydrogen bonds to the central $[Mg(H_2O)_6]^{2+}$ cation are shown in turquoise. Individual $[Ni(notp^{tfe})]^-$ species adopt the Λδ-*RRR* and Δλ-*SSS* OC geometries. Carbon-bound hydrogen atoms are omitted for clarity.

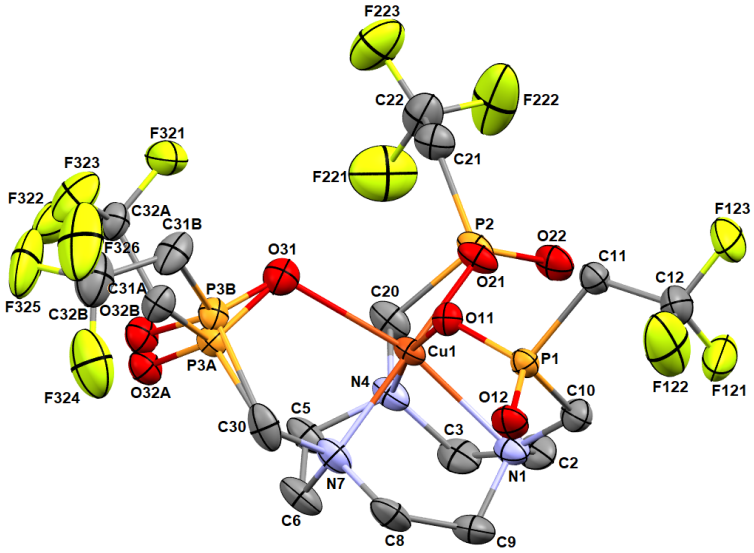

Figure S41. Molecular structure of $[Cu(notp^{tfe})]^-$ anion with the Λδ-*RRR* OC geometry found in the crystal structure of $(NH_4)[Cu(notp^{tfe})] \cdot 3.5H_2O$. Disorder of the pendant arm (attached to nitrogen atom N7) is shown. Hydrogen atoms are omitted for clarity.

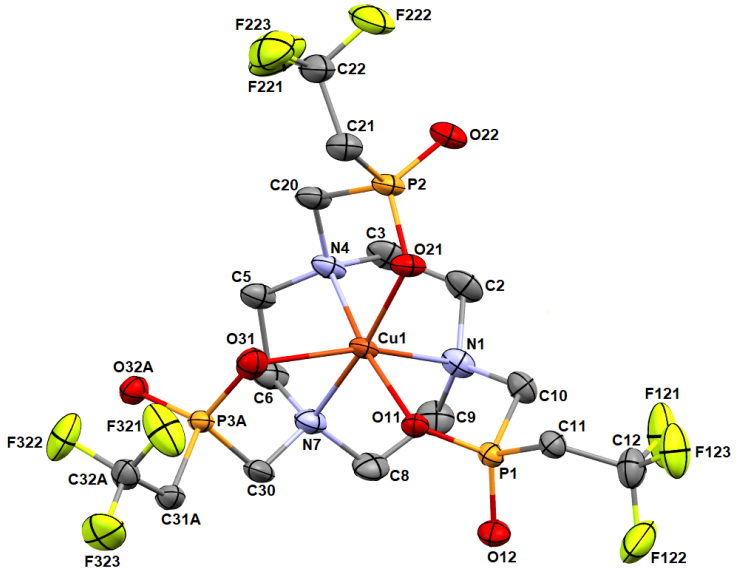

Figure S42. Molecular structure of $[Cu(notp^{tfe})]^-$ anion with the Λδ-*RRR* OC geometry found in the crystal structure of $(NH_4)[Cu(notp^{tfe})]\cdot 3.5H_2O$. More abundant part of the disordered pendant arm (P3A and related atoms) is shown. Hydrogen atoms are omitted for clarity.

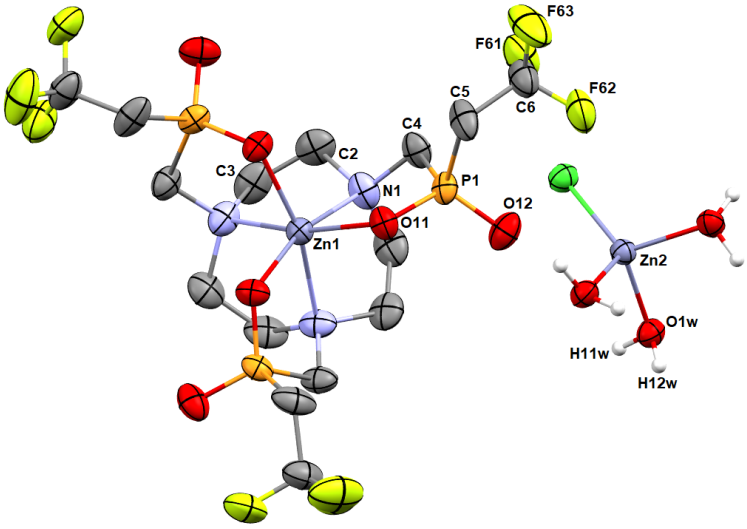

Figure 43. Molecular structure of $[ZnCl(H_2O)_3]^+$ and $[Zn(notp^{tfe})]^-$ fragments found in the crystal structure of $[ZnCl(H_2O)_3][Zn(notp^{tfe})]\cdot 2H_2O$. The complex species $[Zn(notp^{tfe})]^-$ adopt the octahedral Λδ-*RRR* and Δλ-*SSS* geometries (Λδ-*RRR* is shown here). Carbon-bound hydrogen atoms are omitted for clarity.